

Article

Energy Modeling and Techno-Economic Feasibility Analysis of Greenhouses for Tomato Cultivation Utilizing the Waste Heat of Cryptocurrency Miners

Nima Asgari ¹, Matthew T. McDonald ² and Joshua M. Pearce ^{1,2,*}¹ Department of Electrical & Computer Engineering, Western University, London, ON N6A 5B9, Canada² Ivey Business School, Western University, London, ON N6A 5B9, Canada

* Correspondence: joshua.pearce@uwo.ca

Abstract: Greenhouses extend growing seasons in upper latitudes to provide fresh, healthy food. Costs associated with carbon-emission-intensive natural gas heating, however, limit greenhouse applications and scaling. One approach to reducing greenhouse heating costs is electrification by using waste heat from cryptocurrency miners. To probe this potential, a new quasi-steady state thermal model is developed to simulate the thermal interaction between a greenhouse and the environment, thereby estimating the heating and cooling demands of the greenhouse. A cryptocurrency mining system was experimentally evaluated for heating potential. Using these experimental values, the new thermal model was applied to the waste heat of the three cryptocurrency mining systems (1, 50, and 408 miners) for optimally sized greenhouses in six locations in Canada and the U.S.: Alberta, Ontario, Quebec, California, Texas, and New York. A comprehensive parametric study was then used to analyze the effect of various parameters (air exchange rate, planting area, lighting allowance factor, and photoperiod) on the thermal demands and optimal sizing of greenhouses. Using waste heat from cryptocurrency mining was found to be economically profitable to offset natural gas heating depending on the utility rates and Bitcoin value in a wide range of scenarios.

Keywords: waste heat recovery; greenhouse; cryptocurrency mining; technoeconomics; server farms; sustainable food



Citation: Asgari, N.; McDonald, M.T.; Pearce, J.M. Energy Modeling and Techno-Economic Feasibility Analysis of Greenhouses for Tomato Cultivation Utilizing the Waste Heat of Cryptocurrency Miners. *Energies* **2023**, *16*, 1331. <https://doi.org/10.3390/en16031331>

Academic Editor: Pavel A. Strizhak

Received: 8 January 2023

Revised: 14 January 2023

Accepted: 23 January 2023

Published: 27 January 2023



Copyright: © 2023 by the authors. Licensee MDPI, Basel, Switzerland. This article is an open access article distributed under the terms and conditions of the Creative Commons Attribution (CC BY) license (<https://creativecommons.org/licenses/by/4.0/>).

1. Introduction

Our world is struggling with three threatening side effects of population growth. First, food security is one of the critical sustainability indices in a world with about 10% of the population suffering from hunger and 33% living without regular access to adequate food [1,2]. Addressing global famine by relying on conventional food supply policies and technologies will cause an escalation in two other detrimental consequences of population growth: lack of energy and climate destabilization. According to the 2019 Report of the FAO on Food Security and Agriculture [3], 30% of total global energy consumption is attributed to the food chains, which contributes to 19–29% of total annual global greenhouse gas (GHG) emissions and thus the concomitant global warming (13% is occupied by the agriculture [4]). Hence, employing more efficient food production strategies and technologies can contribute to confronting these three coupled challenges of global food, energy, and environmental crises.

One solution is to meet the food requirements of people living in upper latitudes to extend the growing seasons there to provide diversified fresh, healthy food. Greenhouses are a popular solution because the greenhouse (GH) enclosure allows the operators to manipulate and thus optimize the environment inside in which crops will grow, and the greenhouse protects crops from the harsh environment outside, making it feasible for farmers to harvest their desired plants and crops and/or extend the growing season [5]. On the other hand, greenhouses are major energy users (and, with the current energy mix, also

major GHG emitters). For example, in the Netherlands, greenhouses accounted for 79% of energy consumption in the agricultural sector, even though they occupied only 0.5% of the agricultural lands [6]. Canada is one of the northern countries with cold climates, where the greenhouse industry is a major economic contributor providing 1.8 billion CAD in farm gate purchases and 1.4 billion CAD in exports in 2020 [7]. In these northern climates, however, greenhouse heating accounts for 10–35% of the total production costs attributed to the greenhouse [8]. Accordingly, efficient approaches must be taken into consideration for heating the greenhouses to mitigate energy use and GHG emissions while still enabling local food to be produced economically.

One approach to doing this is the use of industrial symbiosis, which is a well-known method to achieve more efficiency and sustainability in production. In this case, the agricultural operations (e.g., soil heating and thermal management of greenhouses and animal shelters) can benefit from the low-temperature waste thermal energy of industries [9]. Most of the available waste heat from global industry is not used. For example, in the U.S., about 75% of the primary energy supply is rejected into the ambient as low-grade waste thermal energy [10]. Therefore, waste heat represents an important opportunity for greenhouse thermal energy supply, especially in cold regions [11]. Furthermore, agricultural-industrial symbiosis encourages local farmers, investors, entrepreneurs, and political decision-makers to invest in the local production of crops, vegetables, and fruits, which will result in a significant reduction in costs related to importing these products [12]. Economics generally governs if an industrial symbiosis project is feasible.

The economic feasibility of waste heat recovery (WHR) strategies in greenhouses has been studied by many researchers [13–17]. Overall, it has been concluded that since heating costs represent a great portion of the overall costs of greenhouses, the WHR is beneficial for greenhouses, especially in winter months and/or for extreme northern climates. One of the fundamental limitations, however, to WHR for greenhouses is the co-location of the heat source. A limited number of studies have been carried out by scientists on the waste heat deployment of data centers (DCs) and server racks in greenhouse heating sectors [18–21]. This research is primarily case studies whose results cannot be generalized for a wide range of applications. Moreover, they have not implemented an economic analysis to determine the profitability of the DC–GH symbioses. The reliable experimental measurements applicable for all future studies, along with the comprehensive mathematical methodology for greenhouse modeling, have also not been carried out in any of these works. In contrast, all these gaps have been addressed in the present work. Furthermore, there are no studies in the literature on the application of cryptocurrency miners' waste heat recovery for residential or greenhouse heating purposes.

Therefore, this study aims to fill these knowledge gaps. First, real-time experiments are conducted on cryptocurrency miners to determine their total waste heat dissipation capacity. Secondly, a quasi-steady state model is employed to simulate the thermal interaction between a greenhouse and the environment, thereby estimating the heating and cooling demands of the greenhouse. This model has been introduced by Ahamed et al. [8]; however, in this study, some enhancements have been made to the model:

- The effect of CO₂ supply furnaces has been ignored to propose a model for net-zero applications.
- A more reliable supplementary lighting model has been introduced for the quasi-steady state approach.
- Different greenhouse sizes (domestic, semi-commercial, and commercial) are developed considering only heat from miners of different operation sizes (an individual miner, a DIY mining container with 50 miners, and a commercial mining container with 408 miners).

This new model was then applied to the waste heat of the three cryptocurrency mining systems, contributing to optimally scaled greenhouses in six locations in Canada and the U.S.: Alberta, Ontario, Quebec, California, Texas, and New York. The economic profitability of these plans has also been evaluated by comparing the costs associated with

the three mining systems and the costs of a conventional natural gas heating system. A comprehensive parametric study was then used to analyze the effect of various parameters (air exchange rate, planting area, lighting allowance factor, and photoperiod) on the thermal demands of greenhouses and, thus, their optimal sizing.

2. Background

This section will provide information on, first, the advantages of greenhouse applications of waste heat recovery (WHR) from the external industrial/residential/commercial sectors and, second, on the energy use in cryptocurrency mining.

2.1. Waste Heat Recovery Strategies Applied to Greenhouses

The technical feasibility of WHR strategies in greenhouses has been carefully studied. For example, Kozai [22] analyzed a greenhouse heated by hot water thermally enhanced through a heat pump, the engine's jacket water, and the engine's exhaust gases. About 70% of the waste heat energy of the engine could be recovered by this system. The recovered energy provided 25% of the greenhouse's thermal demand. The remaining 75% was met by the heat pump. In another work conducted by Chinese et al. [23], the waste heat flow from a newly established waste-to-energy (WTE) plant in northeastern Italy was transported to a 6000 m² greenhouse within a distance of 100 m from the plant. The cooling water of the condenser of the Rankine cycle-based power plant, operated by waste incineration, was directed to the greenhouse. Increasing the greenhouse surface led to an increase in the savings of fuel oil consumption rate under all ambient circumstances. Accordingly, the greenhouse gas emissions have been reduced compared to a case heated by traditional greenhouse heating technologies. Denzer et al. [11] conducted a case study on a 3-acre greenhouse heated with the available waste thermal energy of the Western Sugar Plant in Lovell, Wyoming, during the winter. This plant was discharging hot water at a temperature of 46 °C, and it could be cooled to 26.7 °C before it was discharged to the river. A water-to-air heat pump has been employed to meet the heating demands of the greenhouse. The feasibility analysis demonstrated that the amount of heat rejected from the Sugar Plant would be sufficient to supply the greenhouse. An artificial intelligence (AI) algorithm was employed to provide an infrastructure for communication, gathering data from sensors, etc., in order to model the temperature distribution of a greenhouse under the influence of a WHR system [24]. The residual thermal energy of power plants was managed to operate a solar-assisted heat pump, thereby meeting the heating demands of four 300 m² greenhouses with different crops. As the result of implemented case study, the average energy consumption rate of four greenhouses has been reduced by 30.68% by applying the CHP (Combined Heat and Power) system. The waste heat recovery potential of a paddy straw bale combustor for a 100 m² greenhouse in Ludhiana, India, was investigated through both CFD analysis and a conventional heat transfer model [25].

The economic viability of establishing a greenhouse operating with the waste heat of a flat glass manufacturing plant has been carried out by Andrews and Pearce [13]. Two natural gas and waste heat greenhouses were compared, considering their basic costs to be equal. A total of 5.3 MW out of 11.3 MW of flue gas was recoverable and considering a backup system for the greenhouse, a 3.9-acre greenhouse could be supplied by the waste heat of the manufacturing plant. The greenhouse yield was 735 tons of tomatoes, with an economic value of USD 1.3 million per year. In most cases, the net present value (NPV) of waste heat greenhouse was lower than the natural gas greenhouse, and, considering the natural gas burner as the required CO₂ supplier, this difference became much greater. The feasibility analysis of power plant waste heat utilization in large-scale horticultural plants in three different areas of Korea has been carried out by Yu and Nam [16]. A waste heat recovery system composed of a heat pump, heat storage tank, and heat pipes was designed for each area. It was concluded that the waste energy of power plants is sufficient for the heating supply of each horticultural area so that about 7.4–20% of power plants' reserved energy can afford the thermal demands of the areas. Additionally, from

an economic aspect, using the WHR system instead of the diesel boiler resulted in an 83% reduction in annual operating costs. The energy–economic feasibility and environmental impacts of a project to establish a 1 ha greenhouse (for tomato and cucumber cultivation) supplied by the waste heat of the industrial unit of di-ammonium phosphate production have been studied by Fguiri et al. [17]. The results of this project were compared to a basic case in which natural gas meets the thermal need of the greenhouse. The NPV for the tomato greenhouse was calculated to be 1,127,327 DT (eq. USD 346,000) and 1,293,427 DT (eq. USD 397,000) for the cucumber greenhouse. This proposal could save 746 teq CO₂ compared to the basic case. The technical and economic possibility of the utilization of waste heat from lignite-fired power plants in Greece has been assessed in order to propose an industrial-agricultural symbiosis [14]. The results showed that warm water use in the greenhouse was more economical than conventional fossil-fueled heating systems. The positive impacts of a CHP and CCHP (combined cooling, heating, and power) design on the thermal characteristics of greenhouses and their economic affordability have been evaluated by Tataraki et al. [15]. The study found that the CHP design had an economic advantage over the conventional natural gas boiler, and moreover, the energy-saving ratio was higher for tomatoes in northern locations.

Iddio et al. [26] show that 30% of the world's produced food perishes in transit since the food production centers are usually far from the selling centers. Introducing waste heat-operated greenhouses inside of the cities or in the suburbs could reduce this waste. An urban-centric retail-greenhouse complex was designed for the climate of Calgary, Canada [27]. The heating, ventilation, and air conditioning (HVAC), energy supply, and lighting systems of this complex were optimized, and the waste heat exchange between the two buildings of the complex, along with the solar photovoltaic system, have been considered to improve the energy efficiency of the system and achieve the net-zero energy state. Of the overall energy consumed by the complex, 35% was attributed to heating, and 32% was for refrigeration. Moreover, by considering the on-site solar energy source for the complex, they could sell the excess power energy to the grid during the spring and summer months. In the late fall and winter months, however, they had to buy electricity from the grid. About 130 MWh of waste heat was recovered from the refrigerator's condenser in retail to be used in the greenhouse for space and water heating. The synergetic influence of the airflow exchange of a rooftop greenhouse and an office building HVAC system in a Mediterranean climate has also been studied [28].

The primary challenge of all of these types of systems is the planning needed to couple a waste heat source with a greenhouse. What is needed is the scalable system of a mobile heat load to supply waste heat for greenhouses. One source of waste heat that may be appropriate is data centers and IT infrastructure, including cryptocurrency miners.

2.2. Data Centers and Cryptocurrency Mining as a Source of Waste Heat

Data centers and server racks can be emerging source of waste heat [29]. According to recent advancements in data science and IT technology (e.g., high-tech computers, smart cloud-connected systems, Internet of Things (IoT), and cryptocurrency mining), a considerable portion of global energy consumption is attributed to the data center sector with a value of 3% [30]. Hence, employing useful WHR strategies not only meets the cooling demands of data centers, but can also provide the heating requirements of nearby applications. One simple application of data centers' waste heat is in space heating, named the "Data Furnace" [31]. In the experimental study conducted by Pervilä et al. [19], the growing season of chili pepper was extended by employing a rooftop garden in Helsinki, Finland, and heating it with the waste heat of a servers rack. This server rack could cover the thermal demand of the greenhouse even in the cold seasons. Liu et al. [32] estimated an economic saving of USD 280–325 per server per year when data centers' waste heat was utilized in U.S. residential sectors. The model developed by Sandberg et al. [18] indicated that a 1 MW data center could meet the thermal demands of a greenhouse with a height of 4 m and length of 17 m if the ambient temperature became −30 °C. The operation

of two greenhouses (2000 and 10,000 m²) under two scenarios (partial-year production without grow lights and full-load production with grow lights) has been simulated for enhanced food self-sufficiency using the waste heat of a 1 MW data center in Northern Sweden [20]. The larger greenhouse was a better alternative than the smaller one since it could benefit from more heat recovered and produce less expensive tomatoes (its cost under partial and full-year production was 2.02 and 1.80 EUR/kg (1.97 and 1.75 USD/kg, respectively) for small scale and 1.88 and 1.49 EUR/kg (1.83 and 1.45 USD/kg, respectively) for large scale greenhouse). From the sustainability perspective, the small-scale greenhouse was a better choice since only 10.3% and 2.1% (in partial-year and full-year scenarios, respectively) of its heating demand must be provided by an additional heat source. Cáceres et al. [21] proposed three scenarios to increase food self-sufficiency for three different-sized data center-greenhouse symbiosis in Sweden. These three scenarios were based on three different-sized data centers (small, medium, and large).

Although there is no peer-reviewed article about the WHR of cryptocurrency miners in the literature, all the above-mentioned solutions can be potentially considered as WHR strategies in mining centers since they are analogous to data centers in general [33]. To provide some insight into this, the basic concepts of cryptocurrency and why cryptocurrency mining devices dissipate huge amounts of waste heat are summarized to explain why they can be used as a heating source like data centers.

Traditional currencies primarily take the physical form of notes and coins to be used as a medium of exchange for goods and services in the economy. Third-party entities like Central Banks govern traditional currencies to control supply through monetary policy [34]. Electronic forms of currency can be centralized (regulated by legislation and controlled by a legal organization like banks) or decentralized. Cryptocurrencies are decentralized digital currencies encoded electronically utilizing cryptography to verify transactions and record them on a distributed open-source ledger known as a Blockchain [35,36]. Following the 2008 global financial crisis, Bitcoin was conceived as the world's first cryptocurrency [37]. Bitcoin has gained significant attention from investors as it reached a market cap of USD 1.15 trillion in 2021, with 89 million registered unique Bitcoin wallets on Coinbase [38]. There is a fixed supply of 21 million Bitcoins to prevent issues of inflation [37]. Blockchain is the underlying digital infrastructure upon which cryptocurrencies such as Bitcoin operate, which supports a peer-to-peer digital payment system that has no regulating or central issuing authority [35,37]. It is a public ledger that permanently records and stores all transactions on a cryptocurrency's network using an immutable cryptographic signature called a hash [35,39]. This information is shared with each network participant for complete transparency. The decentralized database of transactions is managed by multiple participants, referred to as miners, who use specialized computing equipment to confirm or deny transactions through a process called mining [40]. All transactions recorded are irreversible, individually encrypted, and time-stamped to ensure security. Transactions are bundled in data structures known as blocks and digitally linked or "chained" together chronologically [35,40]. For the Bitcoin blockchain to function, Miners are tasked with verifying transactions by processing blocks through a system called proof of work (PoW) [41]. This system requires miners to solve mathematical algorithms that are unique to each block of transactions before chronologically adding them to the Blockchain [35,39]. The results are broadcasted to other miners in the network to reach a unanimous consensus and ensure accuracy and security [41]. Miners who solve the algorithm first and encrypt the transactions contained within the block are rewarded in Bitcoin from the network [35,41]. Thus, the profitability of a miner is positively correlated to the miner's computational power, which is measured in hash rate, that is used to solve the mathematical algorithms. The Bitcoin miners operate using the cryptographic hash algorithm known as Sha-2562 to create unique and immutable hashes to solve each block and add it to the blockchain [42]. Miners will invest in specialized hardware to increase their computational power (hash rate) for solving blocks to maximize profitability [43]. Miners may also contribute computational power to community mining pools to receive a proportional reward for the amount of

power contributed [44]. This establishes a consistent cash flow for a business and mitigates the inconsistency in block finding. Accordingly, miners with high-tech processors would be required, and as a result, the high-tech miners will consume a considerable amount of electricity. Therefore, the waste heat created by electronic devices and processors of the high-tech mining hardware has the potential to be a useful source of heat for space heating applications.

3. Methods

3.1. Greenhouse Thermal Model

First, a generic thermal model is developed to simulate the greenhouse microclimate. The roof type of even-span (A-roof) is considered for the proposed greenhouses, and an east-west orientation is selected to benefit from the solar radiation on the sloped east/west-facing roofs equally [45]. The tilt angle (β) of 27° is assumed as the standard slope angle for greenhouse roofs for even-span construction [46,47]. Except for the small-scale greenhouse (1st scenario), the construction of all commercial greenhouses is based on the 4-span design. Other standard assumptions were made for the dimensions and the construction materials of the greenhouses, as shown in Table 1 [48]. Thus, the size of the designed greenhouses would be obtained by the variation of their lengths depending on the amount of waste heat available.

Table 1. The constructive properties of the greenhouse [48].

Characteristics	Value
Width ($4 \times$ span width)	30 m
Eave (gutter) height	3.4 m
Cover	3 mm tempered glass
Interior double glazing	8 mm twin wall polycarbonate on sides and gable ends

As the case study, Edmonton, AL, London, ON, and Montreal, QC, in Canada, along with San Francisco, CA, Houston, TX, and Albany, NY, in the U.S. are used, and thus, the required meteorological data (solar radiation, temperature, etc.) are extracted from the publicly accessible NSRDB (The National Solar Radiation Database). Table 2 presents the most updated meteorological data, TMY (Typical Meteorological Year), of London, ON, for the coldest day of the year to be conservative on the performance of the system and ensure year-round productivity [49,50].

Table 2. The coordinates of London, ON, Canada, and the essential meteorological data for the coldest day there [49,50].

Defining Parameters	Value
The coldest day temperature	-22°C
Average deep soil (at 3 m) temperature on the coldest day (T_g)	8.5°C
Longitude (L_{lc})	-81.14°
Latitude (φ)	43.05°
Standard meridian (L_{st})	90°

3.1.1. Major Assumptions for the Quasi Steady-State Model of Greenhouses

The following assumptions were used to conduct the most accurate and also simplified thermodynamic and heat transfer model on a greenhouse microclimate, in which the complex physical and biological phenomena are in process:

- Most common greenhouse crops, such as tomatoes and cucumbers, require a temperature range of around $18\text{--}25^\circ\text{C}$ [51]. Usually, the growth of crops is improved by decreasing the inside temperature at night and increasing it in the daytime [45,52–54]. Hence, the optimal greenhouse temperature for tomato cultivation is considered to be 15°C and 22°C at nighttime and daytime, respectively [54,55].

- The desirable relative humidity range of greenhouse air for the growth of many plant species is 70–90%, so this parameter is considered 80% in this work [53,56].
- Greenhouse inside air is considered to be well-mixed so that the inside temperature would be uniform. The fluctuation of indoor relative humidity is also considered to be negligible [8].
- Radiative heat exchange between walls and roofs is negligible because their temperature differences are not significantly different [57].
- In conductive and convective heat transfer phenomena, it is considered that the greenhouse envelope is wholly covered with transparent material since the non-transparent ridges and bars (metallic structures) make up a minimal amount of the greenhouse envelope surface area [58].
- The planting area is considered to be 70% of the whole floor area (it should be noted that this value ranges from 60% for conventional greenhouses up to 80% for modern greenhouses with moving benches) [53,59].
- All the heat transfer mechanisms are considered to be one-dimensional and in a steady-state mode [8,57].

3.1.2. The Quasi-Steady State Model

Since the indoor temperature and the relative humidity of the modern commercial greenhouses are almost constant, the greenhouse has been considered a lumped system, so the first law of thermodynamics (energy conservation equation) has been applied to the control volume (CV) of the greenhouse based on the quasi-steady model (GREENHEAT) of Ahamed et al. [8]. In this model, the balance equation between all the heat transfer processes has been implemented for each hour of the day due to the availability of hourly solar radiation data. A schematic illustration of the heat sources and sinks in the greenhouse under study is shown in Figure 1.

$$Q_{net} = Q_{source} - Q_{sink} \quad (1)$$

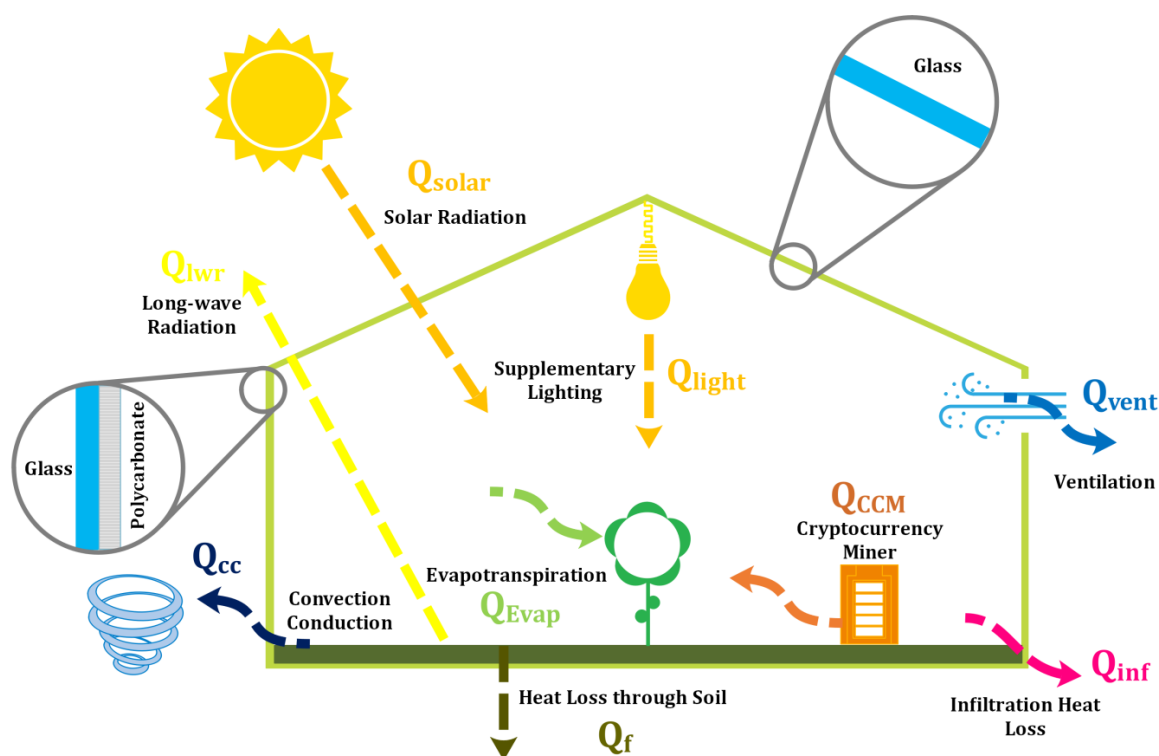


Figure 1. The schematic illustration of the heat sources and sinks in the greenhouse heated with a server or cryptocurrency miner.

The negative value of Q_{net} reveals that there is a heating demand in the attributed hour, and the positive value stands for the cooling demand in the greenhouse. Equation (1) can be expanded as the equation below to include the following heat transfer procedures [8]:

$$Q_{net} = Q_{solar} + Q_{light} - Q_{cc} - Q_{airex} - Q_{lwr} - Q_{floor} - Q_{evap}, \quad (2)$$

in which, Q_{solar} and Q_{light} stand for the heat gained through solar radiation and the supplementary lighting system, respectively. Moreover, indices “ cc ”, “ $airex$ ”, “ lwr ”, and “ $floor$ ” represent the thermal losses through the conduction and convection from the walls and the roof, air exchange, long-wave radiation from the floor, and conduction from the floor, respectively. Q_{evap} is the thermal loss due to the evapotranspiration of the plants. The detailed mathematical equations of each heat transfer mechanism are elaborated in Appendix A.

The greenhouses are designed with respect to the number of their heating demands, which can be met by three waste heat scenarios. In other words, the maximum floor areas, in which the waste heat of each miner scenario can compensate for the maximum absolute value of Q_{net} , are resulted. Q_{CCM} in (J) is the amount of heat dissipated by miners per an hour, which can be derived through Equations (3)–(5):

$$Q_{CCM} = |Q_{net}|, \quad (3)$$

$$Q_{CCM} = \dot{Q}_{CCM} \times 3600, \quad (4)$$

$$\dot{Q}_{CCM} = n_m \sum_1^5 \dot{V}_a \rho_a (H_{a,e} - H_{a,i}) \quad (5)$$

where n_m is the number of cryptocurrency miners used for heating. ρ_a in (kg/m^3) and H_a in (J/kg) are the density and the enthalpy of air entering (i) or exiting (e) the miner. \dot{V}_a is the volumetric flow rate of miners’ fans in (m^3/s). The magnitude of the heat wasted through the miners’ side surfaces in terms of convection and radiation is negligible compared with that of fans blowing.

3.2. Cryptocurrency Miner Systems

To generate experimental values for thermal energy dissipation and profitability metrics of a cryptocurrency mining system, an Antminer S17e manufactured by Bitmain was analyzed in three distinct settings. The first scenario analyzed was with an Antminer S17e operating on its own as an individual mining system plugged into a residential basement setting, shown below in Figure 2.

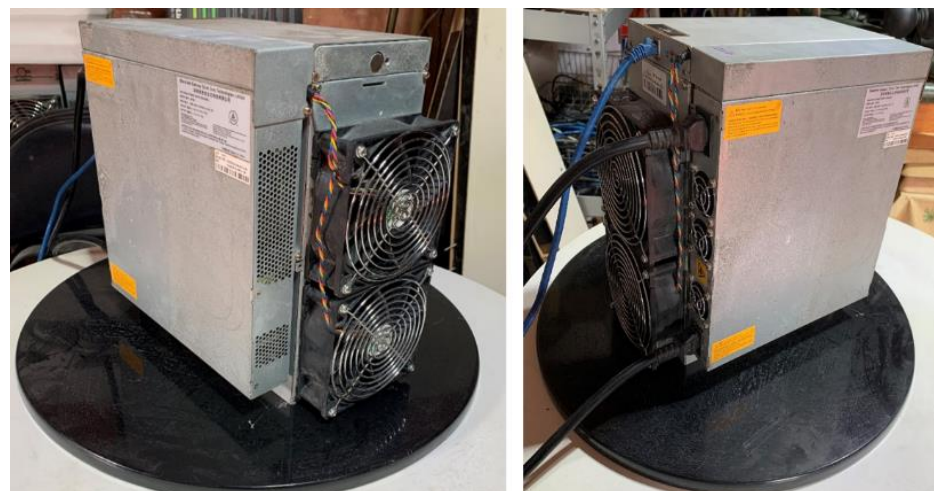


Figure 2. An operating Antminer S17e manufactured by Bitmain. Heat exhaust fans are displayed on the left image with a front-facing view. Cool air intake and power cables are displayed on the right with a rear-facing view.

The second scenario analyzed a DIY cryptocurrency mining container that housed 50 Antminer S17es. The components and associated costs with the transformed shipping container were gathered from cryptocurrency mining company BitMG. The mining container is shown below in Figure 3.



Figure 3. DIY cryptocurrency mining container supporting 50 Antminer S17es. External facing heat exhaust is shown on the left, and the internal mining components are shown on the right.

The third scenario analyzed was a prefabricated commercial-sized cryptocurrency mining container capable of operating 408 Antminer S17es. The MightyPOD mining container from Bit-Ram was selected for analysis and is shown below in Figure 4.

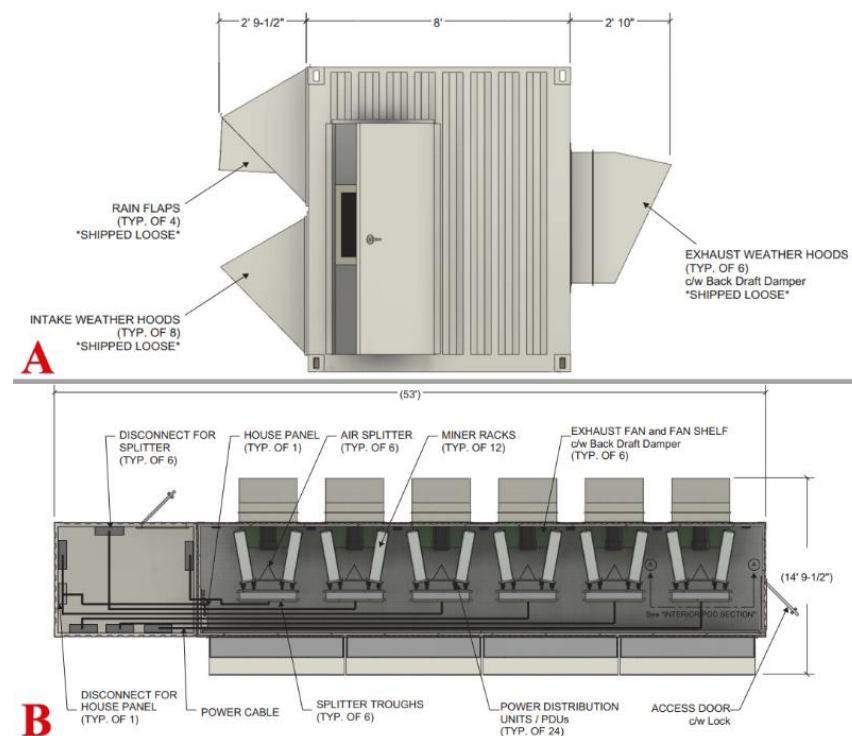


Figure 4. The MightyPOD Prefabricated commercial cryptocurrency mining container from Bit-Ram. This represents the schematic drawing of the MightyPOD container designed to support 408 Antminer S17es. Label (A) denotes the access side view, and label (B) denotes the mining container from a top view [60].

3.3. Cryptocurrency Miner Experimental Measurements

To obtain precise electrical consumption measurements of an Antminer S17e, previous research was done using a PZEM-022 [61] AC digital multi-function meter over a 24 h period [62]. The meter was integrated into each of the Antminer S17e power cables to measure voltage, current, power, energy, frequency, and power factor. This process was replicated over four separate trials on each power cable to ensure measurement consistency.

3.4. Experimental Heat Exhaust

Thermal imaging with a Flir C5 camera [63] was used to identify where heat was localized and exhausted on the Antminer S17e. Thermal measurement probes connected to an Arduino with an SD card were placed on the identified major heat localizations to measure and log this exhaust temperature. Probes 1 and 2 were placed on the top and bottom main Antminer fans, respectively. Probes 3 and 4 were placed on the top and bottom power supply fans, respectively. Temperature measurements were logged every second during four separate 24 h trials to ensure consistency in results.

The three ASIC chips used by the Antminer had their temperatures monitored every hour during the 24-h periods. This was achieved through the Bitmain dashboard accessed by searching the Antminer's IP address in the Firefox browser and navigating to the miner status tab to monitor performance.

3.5. Bitcoin Mining Economic Analysis

The two most important factors to consider when mining Bitcoin are the price of Bitcoin and the domestic electricity rate. Electricity will be the recurring fundamental expense beyond the initial investment into the hardware infrastructure. This makes the decision of where to operate the mining systems critical to reducing this expense by finding the lowest electricity rates. On 5 November 2022, the experimental amount of Bitcoin mined by an Antminer S17e was found to be relatively fixed at 0.098 Bitcoin per year when mined through the community mining pool, Slushpool. The price of Bitcoin valued in USD is the determining factor that most strongly influences profitability. The Bitcoin and USD pairing has historically been very volatile, which introduces considerable uncertainty to an operator's cashflows and their ability to pay the electrical expenses. Under the assumption that an operator is selling the mined Bitcoin daily when received to cover electrical expenses, determining what price of Bitcoin in USD will make a miner profitable will be crucial when deciding to stop or start operating.

Bitcoin Price Sensitivity:

To account for the volatility in the price action of Bitcoin on the profitability analysis, three retrospective USD price levels were selected for analysis since future price predictions can be uncertain. For the most current price data, a retrospective two-year time horizon was chosen to identify the maximum price, minimum price, and average monthly price of USD 69,139, USD 17,600, and USD 37,017, respectively [64].

Geographical Electrical Rate Sensitivity:

Electricity cost is fundamental to the profitability of Bitcoin mining. Variability in electricity rates by geographic location must be accounted for to identify the most profitable location to operate the mining system. In this study, we selected six geographic location and their respective electricity rates to analyze. Electricity rates vary according to the time of day, representing on and off-peak hours. For profitability calculations, we utilized the daily average residential electricity rate and assumed the mining system operated for 24 h a day to account for peak-hour price variability. The locations were Ontario, Quebec, Alberta, Texas, California, and New York, with average residential electricity rates of USD 0.096/kWh, USD 0.054/kWh, USD 0.12/kWh [65], USD 0.13/kWh [66], USD 0.29/kWh [67], and USD 0.20/kWh [68] respectively.

3.6. Simulations

First, the simulation results of the present greenhouse thermal model were validated against the results of similar works. The GREENHEAT model proposed by Ahamed et al. [69] and those of TRNSYS conducted by Choab et al. [54] were selected for comparison. These models have been applied to a hypothetical one-span tomato greenhouse. Accordingly, the validated thermal model was used to estimate the maximum area dedicated for greenhouses potentially heated by the waste heat of three miner scenarios using the experimentally-determined heating potential. The technical feasibility of these greenhouses was evaluated in terms of energy gains and losses. Finally, the parametric study of some useful variables, including air exchange rate, planting area, lighting allowance factor, and photoperiod, were carried out to examine the sensitivities of greenhouse areas to these parameters.

4. Results

4.1. Experimental Electrical Consumption Metrics

The electrical consumption measurements taken from each of the Antminer S17e's two power cables were equal for each variable during separate 24 h trials. The Antminer initiated the powering-on phase for a period between 5 to 30 min. During this phase, it took 6 min for one power cable's power factor, power, and current to reach peak values of 0.99 PF (Power Factor), 1658 W, and 13.84 A, respectively. After 30 min, the frequency became constant at 60 Hz, and the voltage for one power cable fluctuated between 234 V and 244 V. All measurements now stabilized as the power factor became constant at 0.99 PF, power fluctuated between 1618 W and 1634 W, and current varied between 13.50 A and 13.82 A for one power cable. Considering the measurements were identical across both power cables, the total current measurement for the Antminer varied between 27.00 A and 27.64 A, while the power measurement fluctuated between 3236 W and 3268 W. The cumulative energy drawn by one power cable for a 24 h period was measured hourly to be 39.08 kWh and, therefore, 78.16 kWh total for the Antminer, as shown in Figure 5. This equates to a total continuous power draw of 3256 W for the Antminer.

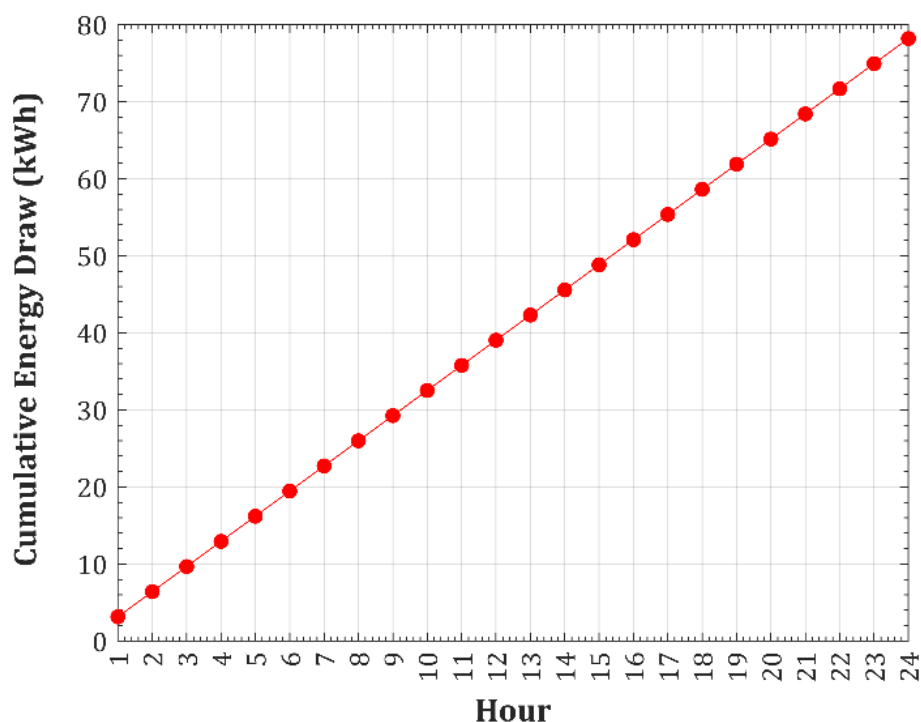


Figure 5. Representative total cumulative Antminer S17e experimental energy draw measurements over a 24-h period in kWh across the two power cables.

4.2. Experimental Heat Exhaust

Thermal images of the Antminer are shown in Figure 6. The temperature data of the heat exhausted through the main Antminer fans measured by probes 1 and 2 are denoted by temperatures 1 and 2 in Figure 7. Temperature ranges are given after temperature data stabilization is achieved 30 min post power-on routine of the Antminer. Temperature 1 fluctuates for the duration of the experiment between the range of approximately 55 °C and 52 °C. Temperature 2 fluctuates between approximately 56 °C and 53 °C. The temperature of the heat exhausted through the power supply fans measured by probes 3 and 4 are denoted by temperatures 3 and 4 in Figure 7. Temperature 3 fluctuates predominately between 43 °C and 32 °C while temperature 4 fluctuates between approximately 37 °C and 31 °C. The Antminer S17e's two main heat exhaust fans are the Nidec UltraFlo W12E12BS11B5-57 model [70] that have the capability of 79.7 CFM (0.03761 m³) for each fan enabling capacity for 159.4 CFM. The two power supply heat exhausts are comprised of three PWM Speed Control Fans 04028DA-12S-AUF-0 [70] that have the capability of 8.58 CFM (0.0040 m³) each for a cumulative 25.74 CFM. Therefore, the Antminer S17e has a total CFM of 185.14 across all heat exhaust fans.

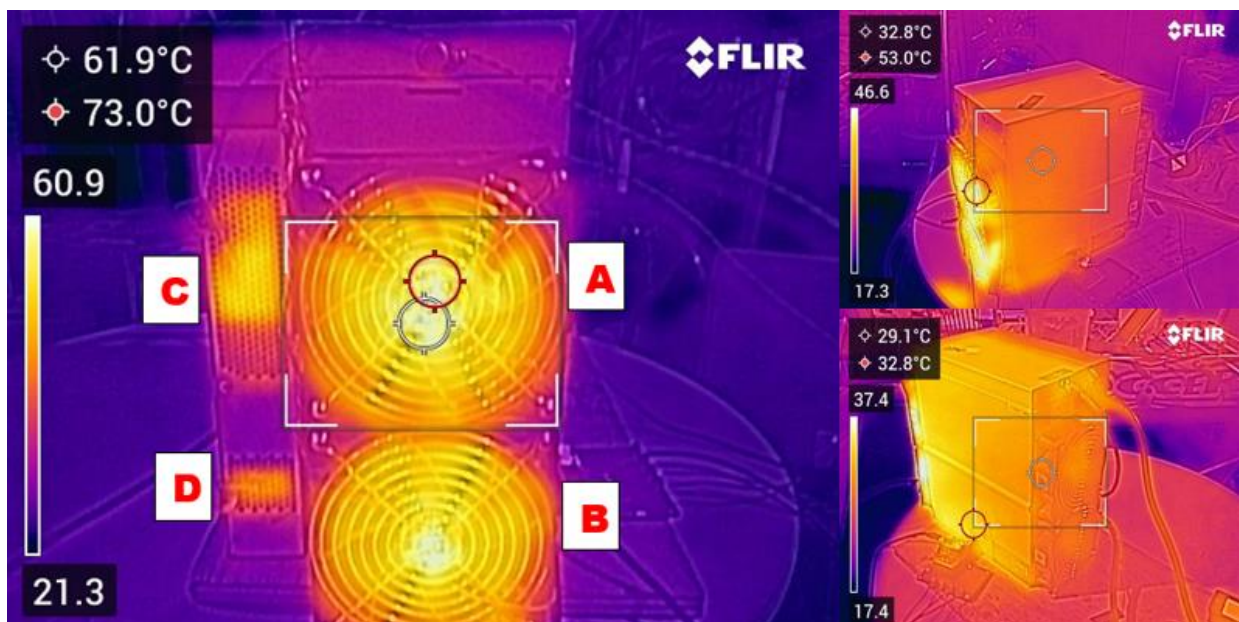


Figure 6. Antminer S17e heat localization thermal images measured in degrees Celsius. Label **A** and **B** denote the Antminer's top and bottom main fans measured by probes 1 and 2, respectively. Labels **C** and **D** denote the Antminer's top and bottom power supply fans measured.

Putting the measured values of temperature and volumetric flow rates in Equation (5), the waste heat of the Antminer is obtained around 3.24 kW, which shows that the power consumed by the miner is almost completely converted to waste heat.

4.3. Experimental ASIC Chip Temperature

Each ASIC chip takes approximately 5 min to reach maximum temperature before stabilizing within a narrow range. ASIC chip 1's temperature fluctuated between 60 °C and 68 °C, while chip 2 and 3's temperature fluctuated between 60 °C and 67 °C, and 64 °C and 73 °C, respectively.

4.4. Greenhouse Simulation Results

As shown in Figure 8, there is a close agreement ($\pm 9.3\%$) between the results of this model and those of the related GREENHEAT and TRNSYS reference models.

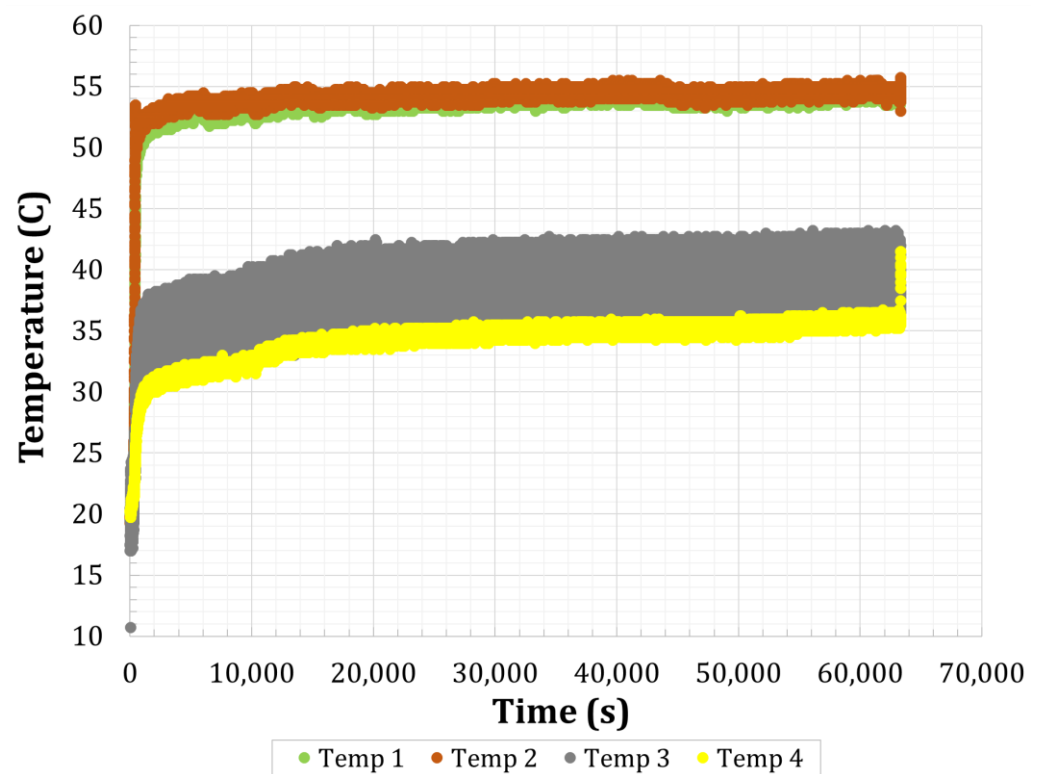


Figure 7. Antminer S17e heat exhaust over a 24 h period measured in degrees Celsius. Temperature 1 refers to heat exhausted from the top main fan of the Antminer. Temperature 2 refers to the heat exhausted from the bottom main fan of the Antminer.

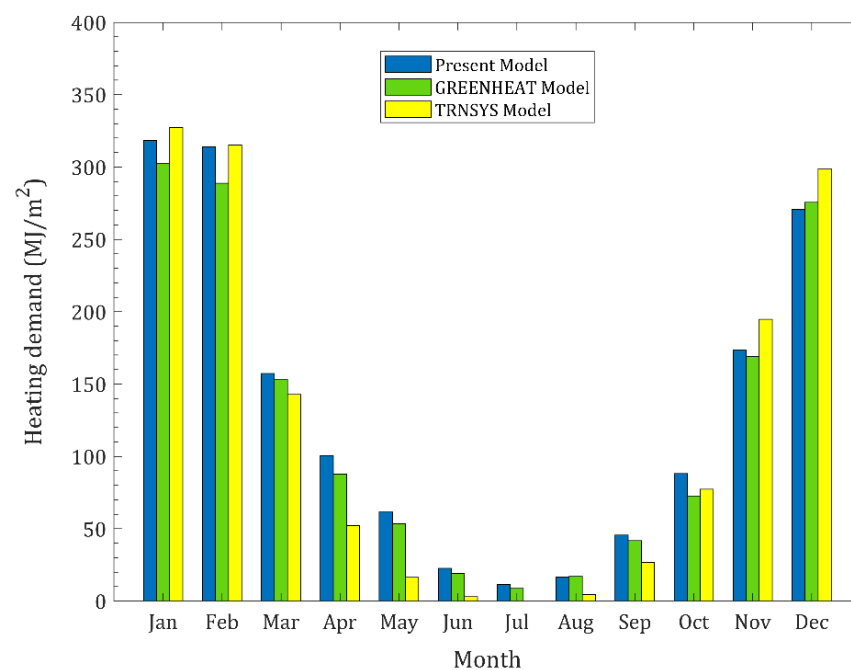


Figure 8. Comparison between the results of the present greenhouse model and those of GREENHEAT [69] and TRNSYS [54].

4.4.1. Technical Feasibility

In this section, the technical feasibility of greenhouse designs has been evaluated considering three miner scenarios (Individual Antminer S17e, DIY Mining Container, and MightyPOD Commercial Mining Container). The maximum sizes of technically feasible

greenhouses have been found considering the maximum heating requirement of each greenhouse to be met by each of the miner scenarios. Table 3 presents the characteristics of the potentially feasible greenhouses in London, ON, Canada.

Table 3. The characteristics of the greenhouses designed for three miner scenarios in London, ON.

No.	Miner Scenario	Number of Miners	Span Dimensions (Width × Length × Height) (m)	Number of Spans	Greenhouse Area (m ²)	Annual Heating Demand (GJ)	Annual Cooling Demand (GJ)
1	Individual Antminer S17e (1st)	1	3.12 × 3.12 × 1.9	1	9.7	22.3	79.9
2	DIY Mining Container (2nd)	50	7.5 × 25.81 × 3.4	4	774.3	1.0×10^3	3.6×10^3
3	MightyPOD Commercial Mining Container (3rd)	408	7.5 × 229.81 × 3.4	4	6894.3	8.3×10^3	2.9×10^4

Table 3 demonstrates that, for the first scenario, the Antminer S17e is capable of providing the maximum heating demand of a small residential or bench-scale greenhouse with an area of 9.7 m². In the second scenario, however, the allocatable area for the greenhouse being heated by 50 miners is 80 times larger (on a semi-commercial scale). In the third scenario, the MightyPOD commercial mining container can meet the heating demand of a 6894 m² commercial greenhouse for tomato cultivation. The technically feasible greenhouses are illustrated in Figure 9.

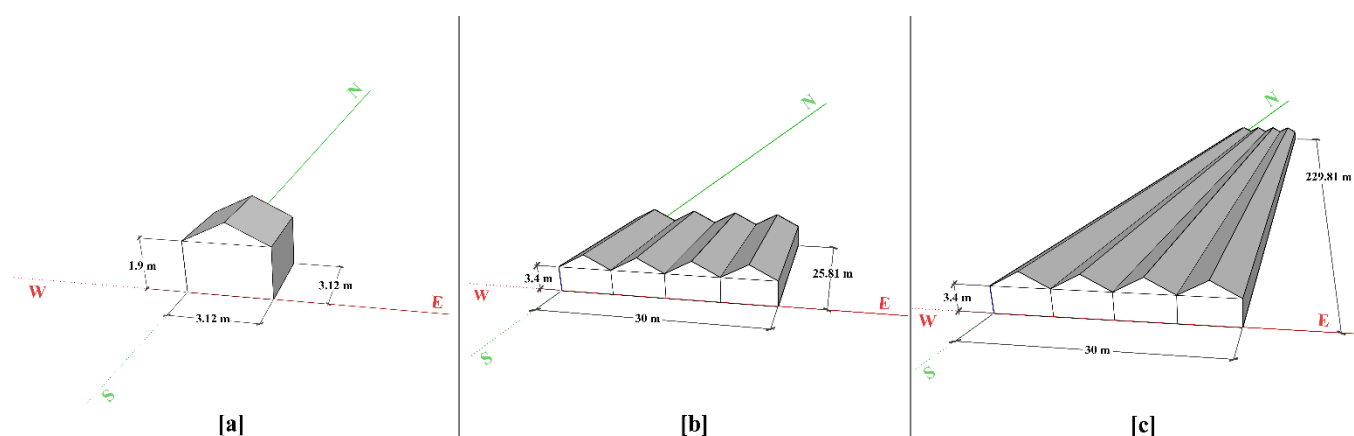


Figure 9. The technically feasible greenhouses for each miner scenario (a) 1st scenario; (b) 2nd scenario; (c) 3rd scenario in London, ON.

All these greenhouses have been designed based on their maximum heating demand on the coldest day of the year in London, ON, which has been selected according to the simulation results of daily heating demand, as shown in Figure 10.

Table 4 corresponds to the characteristics of greenhouses designed under the climatic circumstances of five other locations, including Quebec (QC), Alberta (AL), California (CA), Texas (TX), and New York (NY). Referring to the table's data, it can be deduced that for all three scenarios, it is feasible to design larger greenhouses in the regions with warmer climates (e.g., California, Texas, and New York) and vice versa (e.g., Quebec and Alberta). However, for the southern regions (CA and TX), there is a noteworthy point to discuss. Since the greenhouse sizes have been obtained with respect to their heating demands on the coldest day of the year, the areas dedicated to building the greenhouses in California and Texas are considerably larger than the area obtained for other colder regions. Nevertheless, the annual heating demands of CA and TX cases are less than those of the colder regions (e.g., QC and AL). This proves the capability of the miner waste heat utilization idea in meeting the heating demands of the greenhouses under the worst conditions, thereby leading to designing the largest producible greenhouses.

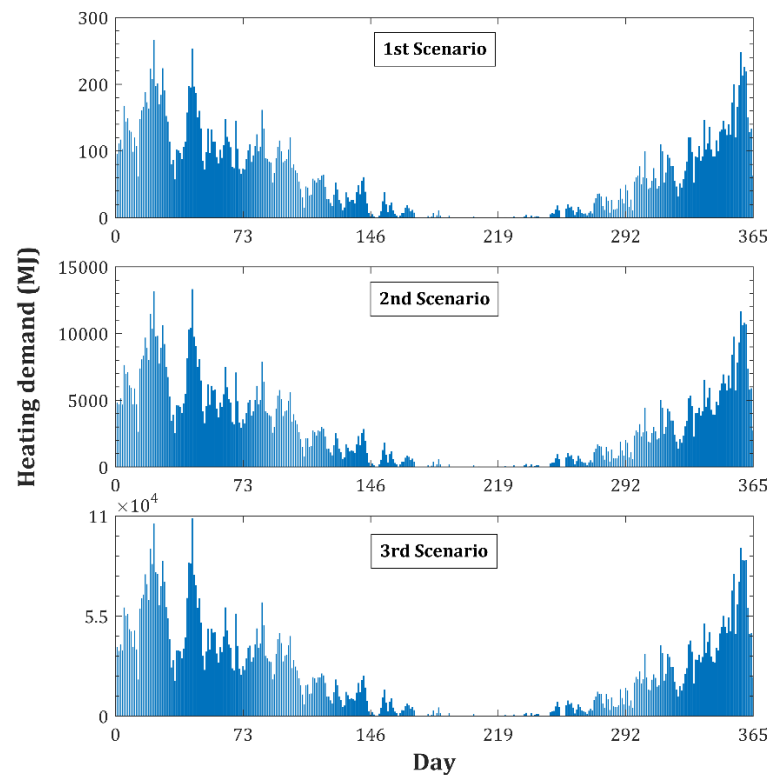


Figure 10. Daily heating demand of the greenhouses in London, ON.

Table 4. The characteristics of the greenhouses designed for three miner scenarios in Quebec, Alberta, California, Texas, and New York.

Region/Miner Scenario	Greenhouse Area (m ²)	Annual Heating Demand (GJ)	Annual Cooling Demand (GJ)
Quebec			
1st	6.5	21.3	55.5
2nd	524.7	1.0×10^3	2.3×10^3
3rd	4887.3	8.1×10^3	1.8×10^4
Alberta			
1st	7.8	25.2	64.5
2nd	640.8	1.2×10^3	2.7×10^3
3rd	5804.7	9.5×10^3	2.1×10^4
California			
1st	79.4	20.4	723.3
2nd	5133.9	1.0×10^3	37.5×10^3
3rd	42,561	8.5×10^3	30.6×10^4
Texas			
1st	38.4	9.9	375.6
2nd	2989.5	0.5×10^3	21.7×10^3
3rd	25,512.6	4.4×10^3	18.1×10^4
New York			
1st	15.8	22.9	122.3
2nd	1217.4	1.1×10^3	5.7×10^3
3rd	10,615.5	9.0×10^3	4.6×10^4

The monthly heating and cooling demands of each greenhouse, along with the contributions of all energy sources and sinks, are extracted and illustrated for London, ON, as follows. This evaluation is required to define the energy sources and sinks with the highest/lowest contributions in terms of MJ and help greenhouse designers pay more attention to the thermal weaknesses of the potential greenhouses. According to Figure 11, it

is obvious that the heating plots have a reversed trend with respect to the cooling plots. The heating demand of all the greenhouses tends to be zero in summer months, and the cooling demands, however, do not approach a zero value even in the cold seasons. This is owing to the fact that even in winter months, during the day, the sunlight radiation provides considerable heating inside the greenhouses. As it is presented in Figure 11, generally, the cooling demands of the greenhouses in all the scenarios are larger numbers compared with the heating demands. This is because of the ventilation submodel that has been used in this study. In order to predict the maximum cooling demands of the greenhouses, natural ventilation has not been considered as a contribution to meeting the cooling demands of the greenhouses.

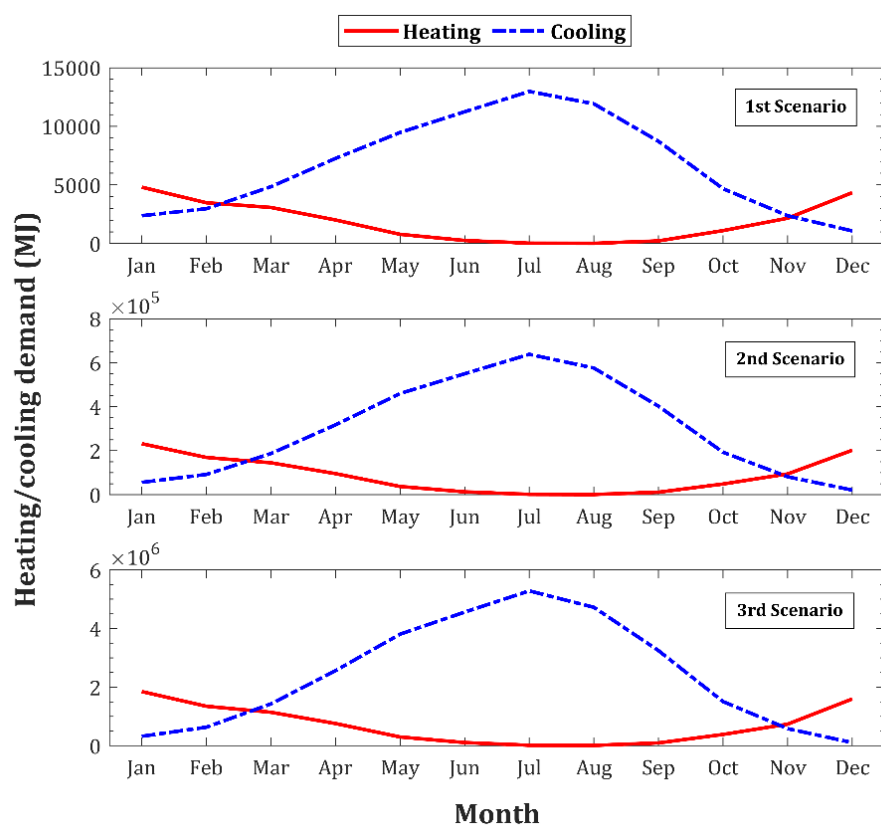


Figure 11. Monthly heating and cooling demands of the greenhouses.

The contribution of all the heating sources, including solar irradiation and supplementary lighting thermal energy, is illustrated in Figure 12. The amount of energy obtained by each greenhouse is almost ten times higher than that of the smaller case. Figure 12 reveals that by increasing the magnitude of the solar energy received by the greenhouses, the contribution of the supplementary lighting system gets smaller since the DLI (daily light integral) acquired by the plants must be in a limited range.

Figure 13 demonstrates the value of heat losses because of the conduction, convection, and air exchange in the greenhouses. The conduction and convection losses from the greenhouse walls and roof represent a considerable portion of all the thermal losses. Hence, designers should pay more attention technically to these loss factors to optimize them as much as possible. It is also clear that the value of heating losses approaches zero by increasing the ambient temperature, and they become negative in July and August. This is because in these months, the outside temperature is higher than the inside temperature while having the maximum difference with it, which makes these heat sinks behave not as a thermal loss anymore, but as a thermal energy source from the greenhouse viewpoint. Conversely, the conduction heat loss through the greenhouse floor is not notable compared

to the other sources. Since the deep ground temperature is almost constant during the year, the magnitude of the heat loss from the soil does not vary significantly.

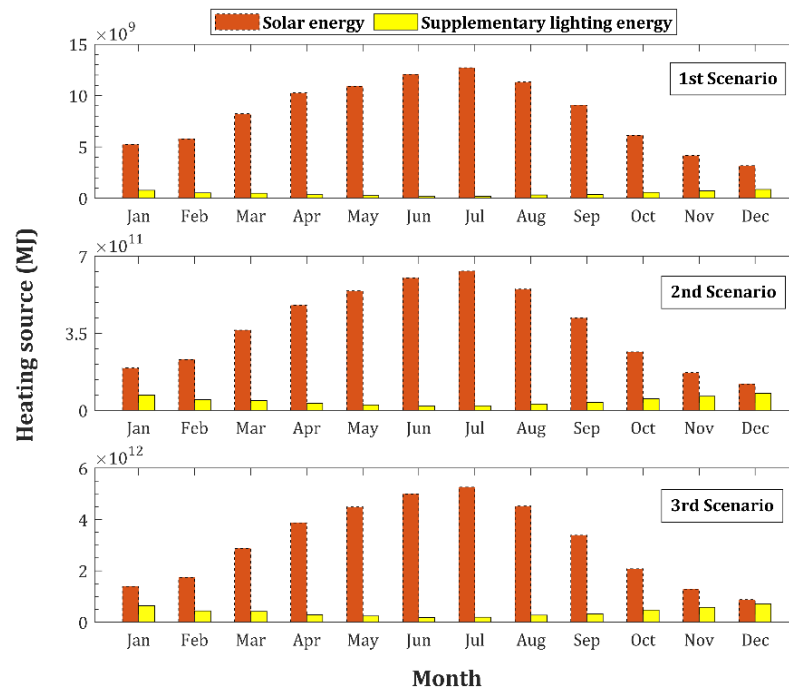


Figure 12. Monthly magnitude of heating sources in greenhouses.

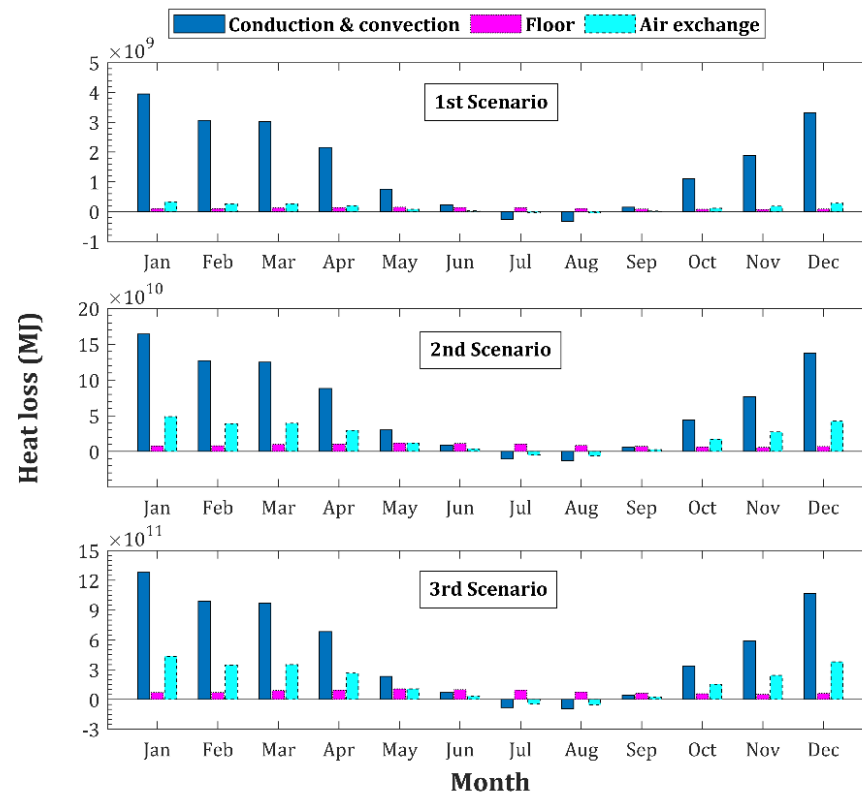


Figure 13. Monthly values of heating losses through the conduction, convection, and air exchange in the greenhouses.

Figure 14 clarifies that the heat loss through long-wave radiation has the largest contribution among all the thermal losses, especially compared with the evapotranspiration loss. Going toward the summer, the long-wave radiation not only causes no thermal losses but also becomes a heat source making the greenhouses' indoor temperatures higher than the desired levels.

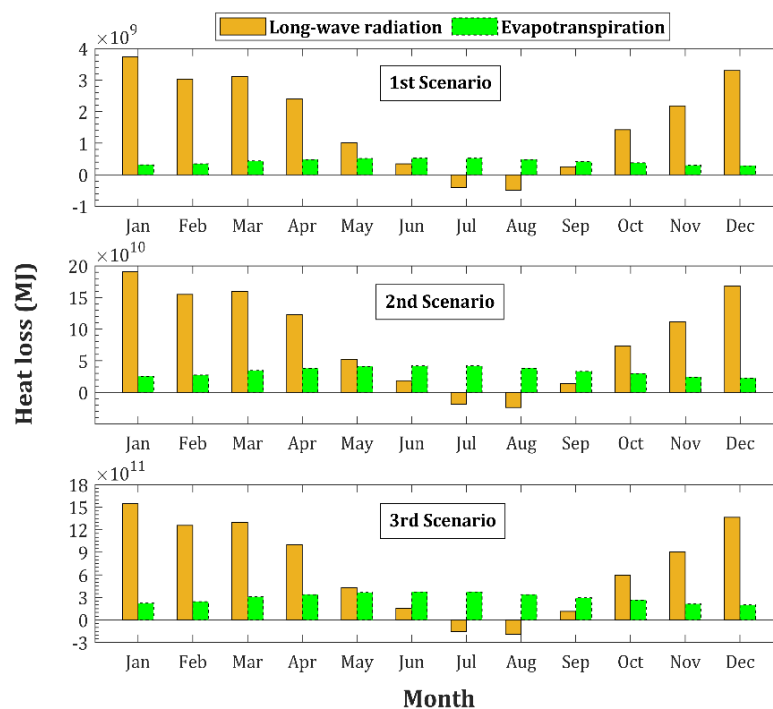


Figure 14. Monthly values of heating losses through long-wave radiation and evapotranspiration.

4.4.2. Sensitivities

In this section, the effect of the variation of parameters on the size of the designed greenhouses and their thermal demands were investigated. It is worth mentioning that the overall trend of objective functions (greenhouse area and heating demands) is the same for all the scenarios; their magnitudes, however, are different. Figure 15 presents the variations of the objective functions under the influence of air exchange rate changes from 0.7 to 1 ACH (Air Change per Hour) as the minimum unavoidable ventilation and infiltration rate in the greenhouses without supplementary CO₂ supply systems (further details and discussion have been provided in Appendix A). As expected, increasing the air exchange rate, the maximum greenhouse area diminishes by about 2.5% in the first scenario and 7% in the second and the third scenarios, respectively. Nevertheless, the annual heating demands of all three greenhouses increase by raising the air exchange rate since the amount of accumulative heat loss through the air exchange increases. Therefore, appropriate measures and considerations should be taken to keep the infiltration and unnecessary ventilation rates as below as possible.

The effect of different considerations for the lighting allowance factor of supplementary lighting systems on the size of the designed greenhouses, their heating and cooling demands, along with the cumulative amount of heat obtained from the supplementary lighting system, have been evaluated, and the results are shown in Figure 16. Although the variations are not considerable, the interconnections between the lighting allowance factor and the objective functions produce useful conclusions. By increasing the lighting allowance factor, the practical power consumption rate of the lighting system is increased, and thus, the greenhouses would be supplied with more thermal energy, which would subsequently increase the area that can be heated by the waste heat of the crypto miners. With an increase in the sizes of the greenhouses, their cooling and heating demands are also

increased. The effect of excess heat supplied by the supplementary lighting, however, outweighs the effect of thermal energy needed because of the enlargement of the greenhouses. As a result, the annual heating demand of all the greenhouses is reduced slightly.

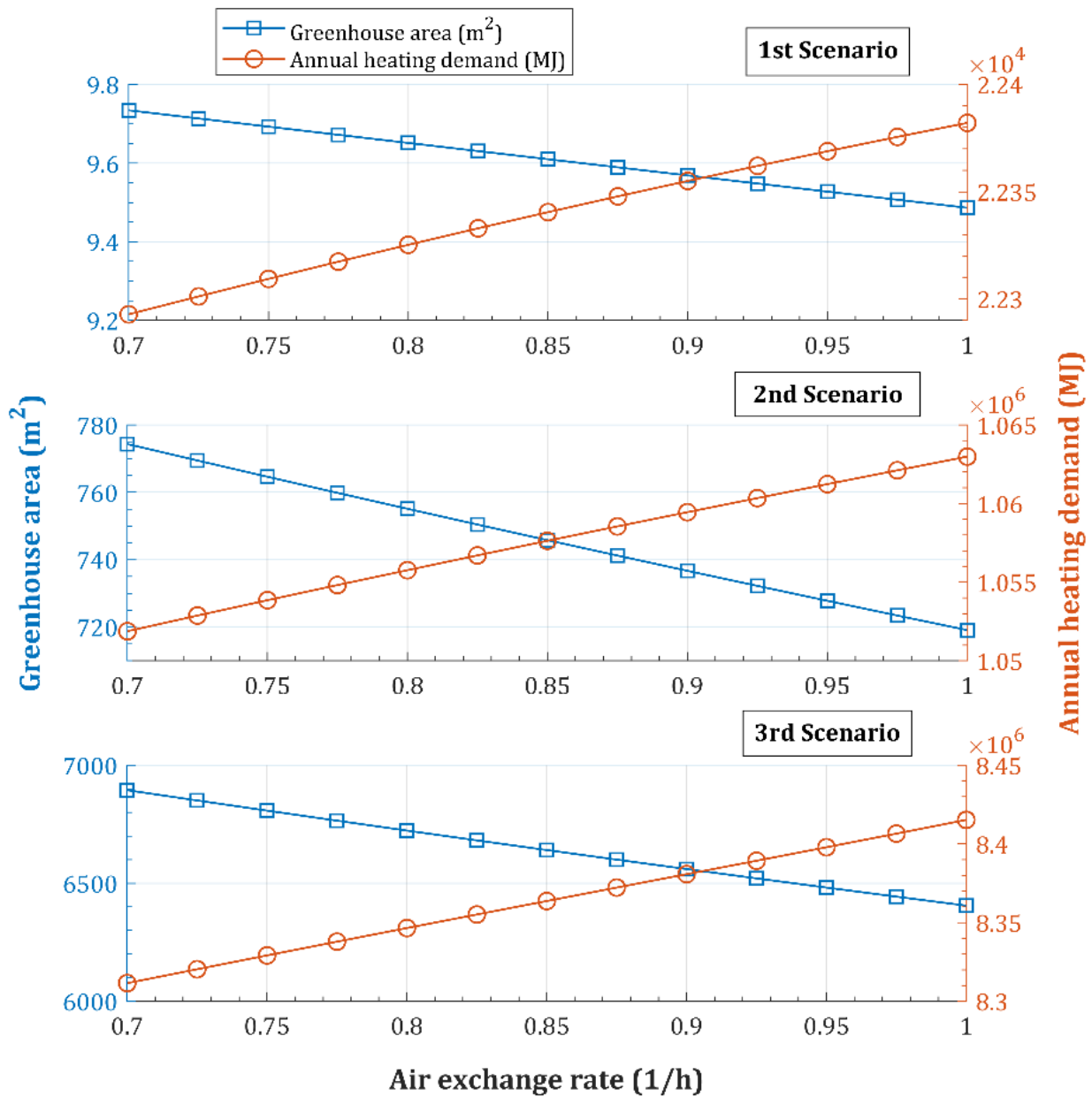


Figure 15. Variations of the greenhouse size and annual heating demand under the variation of the air exchange rate.

The variations in greenhouse sizes with respect to the variation in photoperiod are depicted in Figure 17. It is clear that by increasing the photoperiod, the greenhouse area would be increased up to a maximum, then would tend to decrease. The reason responsible for such a behavior is the interconnection of the effects of increasing the lighting hours and decreasing the number of lights with the rise in the photoperiod, which is more considerable in the small greenhouse. When the photoperiod goes up, it means that the number of lighting hours increases, which leads to an increment in the amount of thermal energy supplied by the supplementary lighting system and subsequently causes the enlargement of the designed greenhouses' areas when there is a fixed source of heat from the miners. Correspondingly, by raising the photoperiod, the number of lights needed to provide the

required DLI can be reduced, which, in turn, reduces the heat supplied by the lighting systems, thereby reducing the sizes of the greenhouses. The maximum greenhouse sizes are achievable within a photoperiod between 17 to 19 h per day.

The planting (canopy) area fraction is the part of the whole greenhouse area that is dedicated to planting. This fraction can be varied between 0.6–0.8 according to the type and applications of the greenhouse. Figure 18 presents the effect of variation of this fraction on the greenhouse sizes and the thermal indices of each greenhouse in separate subplots. By dedicating more area for planting, the amount of heat loss through the evapotranspiration of plants would be increased, which is clear in Figure 18. This increasing trend in evapotranspiration heat loss results in a decrement in the sizes of the greenhouses that can be potentially heated by the miners. Although the reduction in the sizes of greenhouses will cause a reduction in the annual magnitudes of heat losses other than evapotranspiration, the increment of evapotranspiration heat loss outweighs the decrement of these losses, which accordingly causes a slight increase in the overall accumulative heating demands of the greenhouses. On the other hand, the combination of a reduction in sizes and an increment in evapotranspiration heat losses would lead to a considerable reduction in the cooling requirements of the greenhouses.

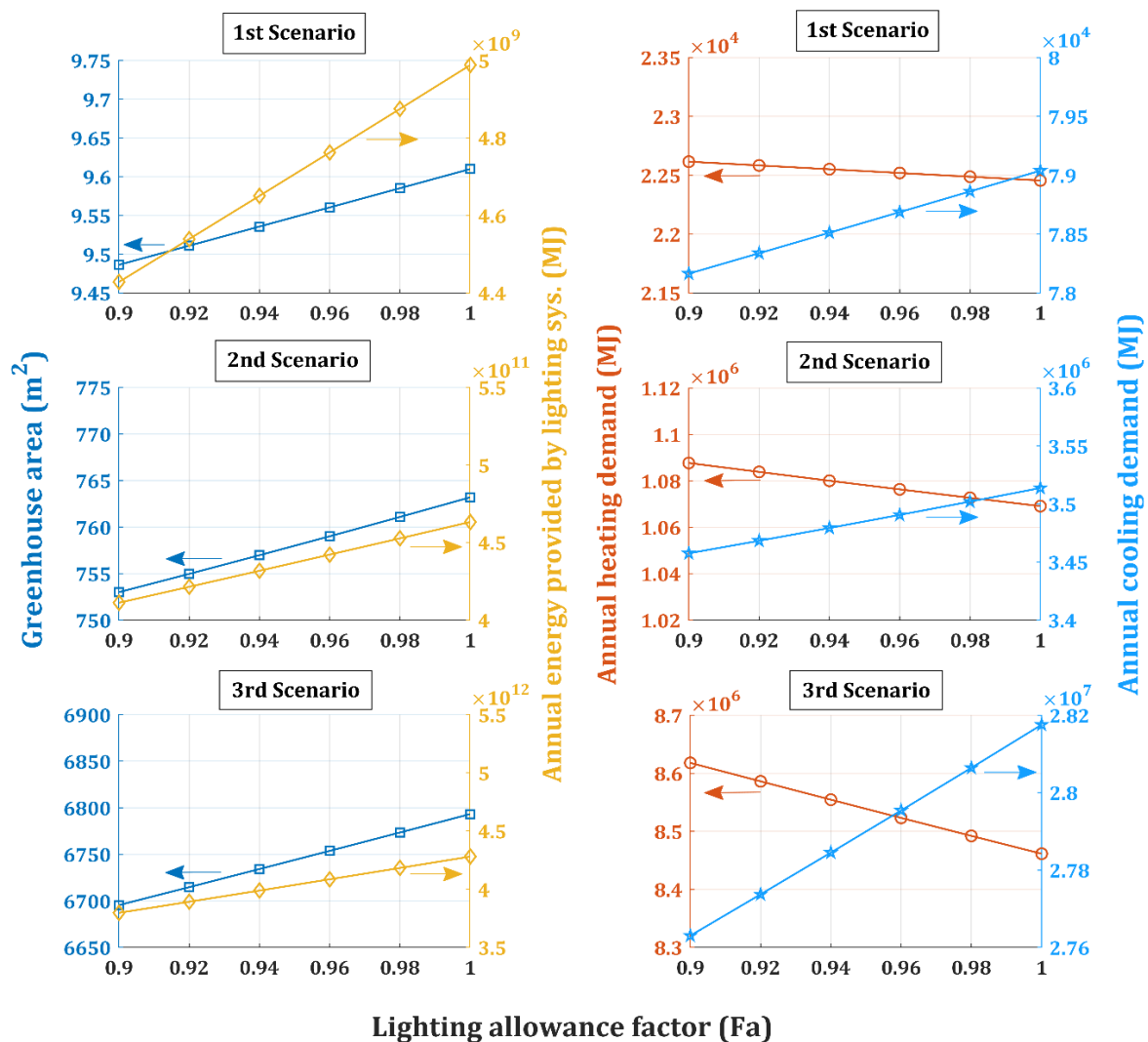


Figure 16. Variations in the greenhouse sizes, annual heat provided by supplementary lighting, annual heating demand, and annual cooling demand under the variation of the lighting allowance factor.

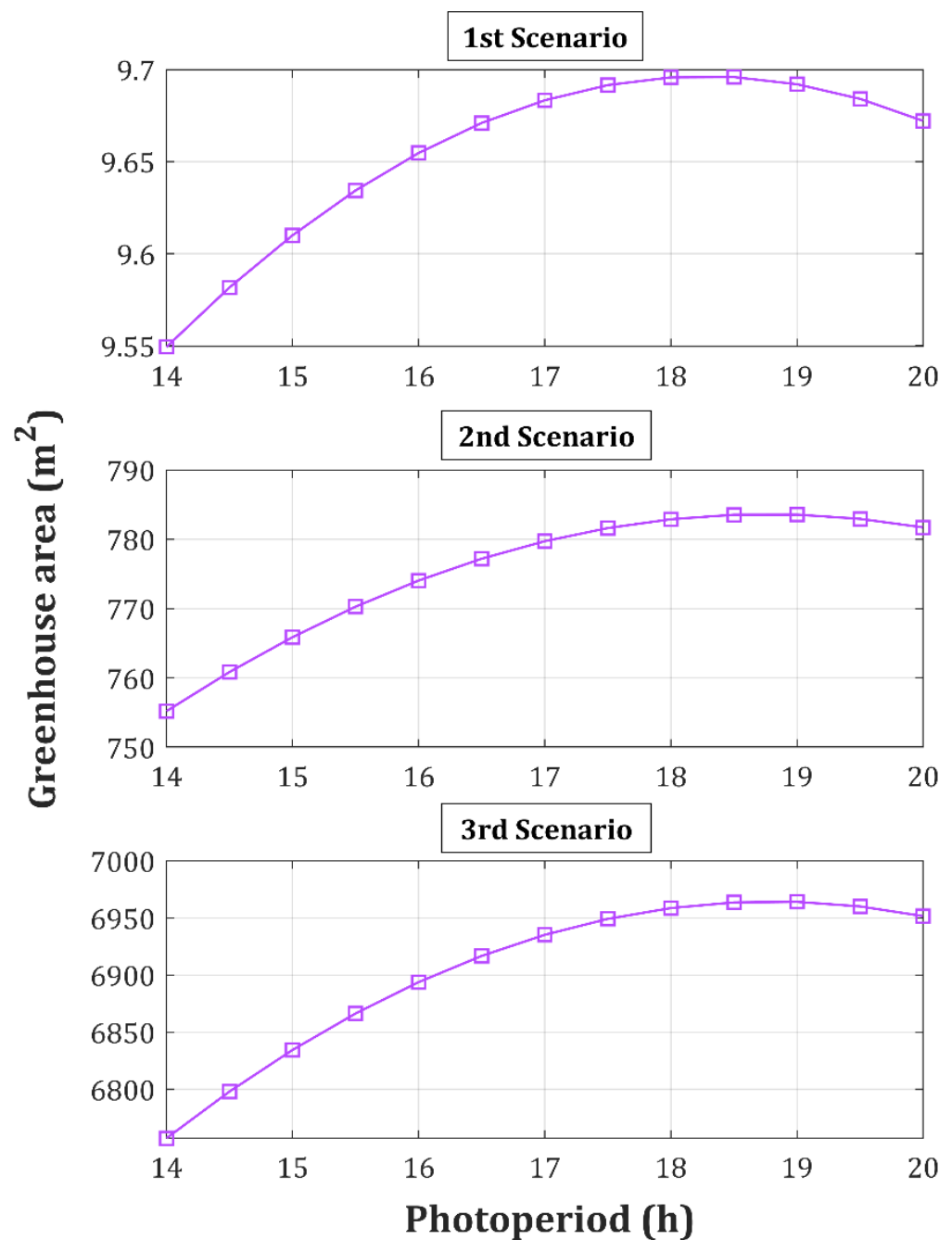


Figure 17. Variations in the greenhouse sizes under the variation in the photoperiod.

4.5. Economic Analysis of Greenhouse Heating

4.5.1. Bitcoin Mining Heat Source

A profitability analysis was conducted when utilizing Antminer S17es to adequately heat greenhouses in six distinct North American locations while mining Bitcoin using the results of the thermal simulation. The three Bitcoin mining systems assessed were an individual Antminer S17e, the DIY mining container, and the commercial MightyPOD container, each capable of heating greenhouse sizes of 9.7 m², 774 m², and 6894 m², respectively in London, ON, as outlined when analyzing technical feasibility. The greenhouse sizes in other North American locations are provided in Table 4. The profitability results of each mining system considered the domestic electricity rates in each location on electricity expense and the price volatility of Bitcoin at the time of sale. A high, medium, and low profitability case was established, corresponding to the Bitcoin price sensitivities of USD

69,139, USD 37,017, and USD 17,600, respectively. The annual profitability results for the individual Antminer S17e are summarized below in Figure 19.

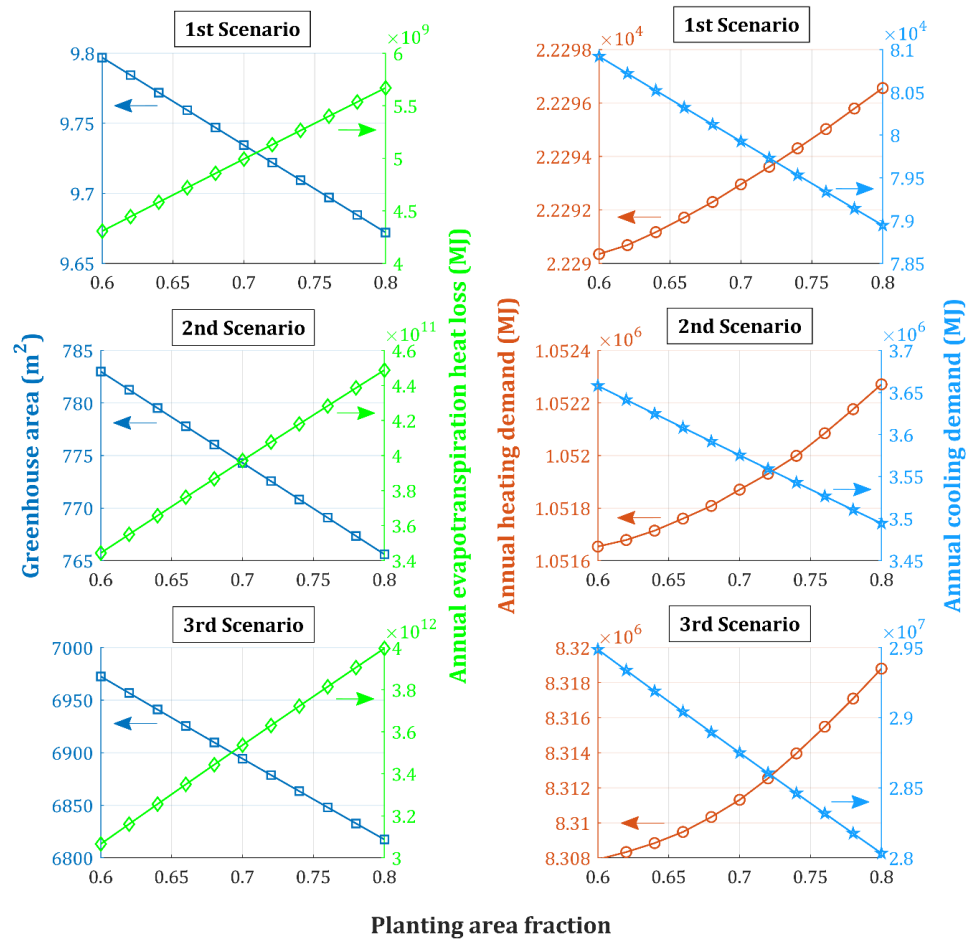


Figure 18. Variations in the greenhouse sizes, annual evapotranspiration heat loss, annual heating demand, and annual cooling demand under the variation in the planting (canopy) area fraction.

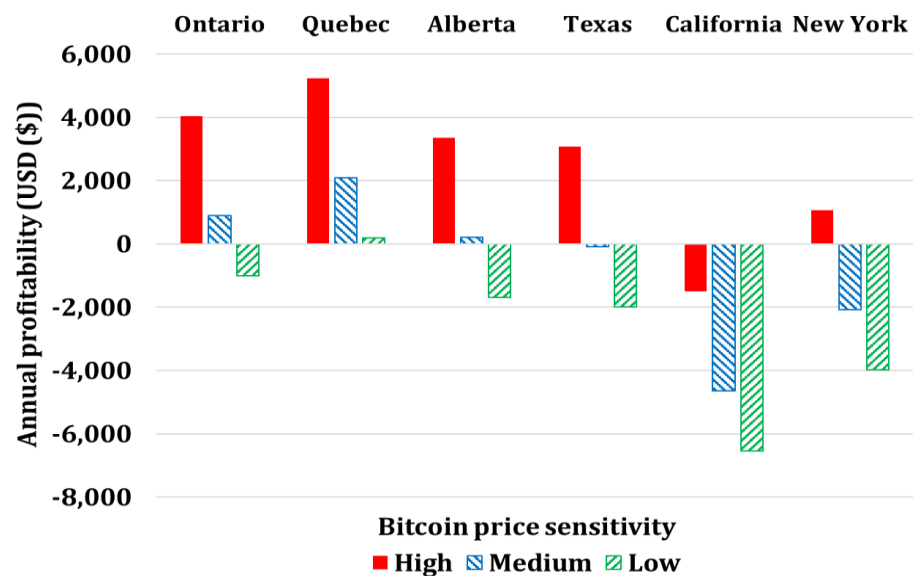


Figure 19. Annual profitability results of operating an individual Antminer S17e in six North American locations measured in USD.

Considering the initial investment of USD 1523 for the individual Antminer S17e, the time required to recoup this investment is summarized for each location below in terms of payback periods in Figure 20.

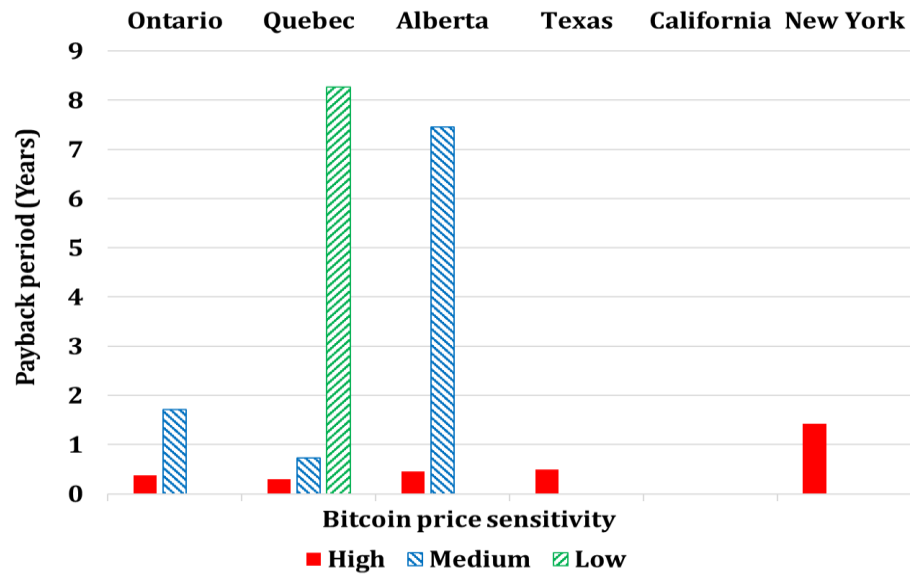


Figure 20. Payback period results from the initial investment for an individual Antminer S17e operating in six North American locations measured in years.

The annual profitability results for the DIY mining container are summarized below in Figure 21.

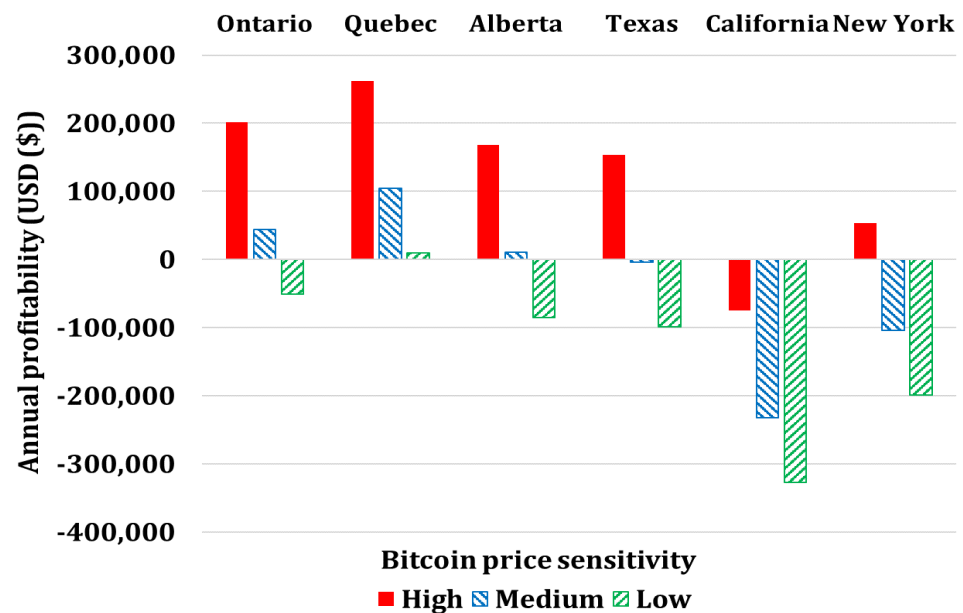


Figure 21. Annual profitability results of operating a DIY mining container in six North American locations measured in USD.

Considering the initial investment of USD 112,584 for the DIY mining container, the time required to recoup this investment is summarized below in terms of payback periods in Figure 22.

The annual profitability results for the commercial MightyPOD container are summarized below in Figure 23.

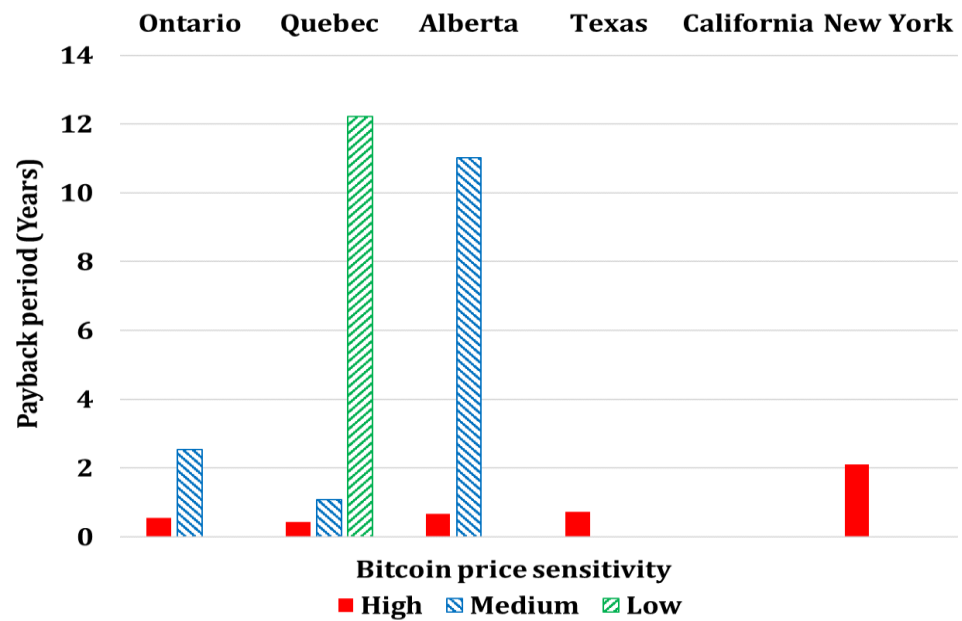


Figure 22. Payback period results from the initial investment for a DIY mining container S17e operating in six North American locations measured in years.

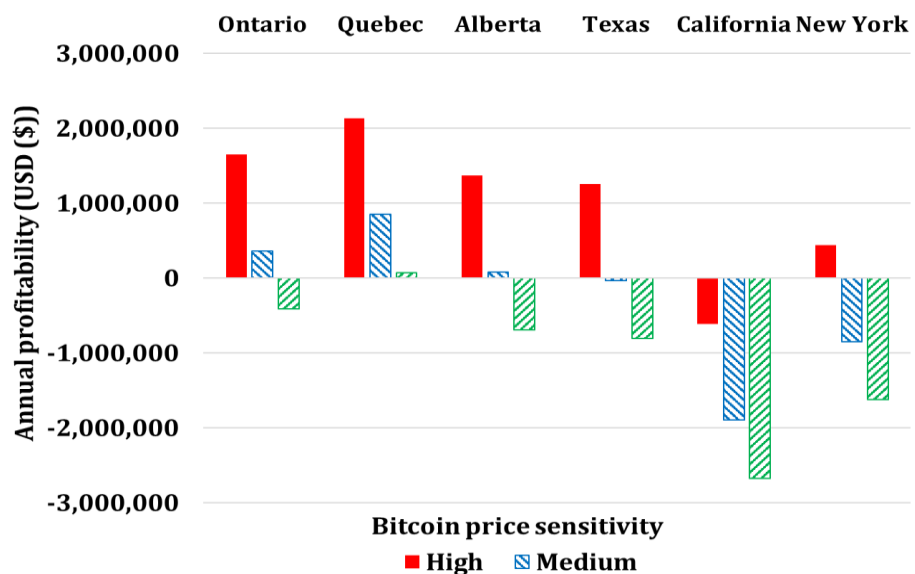


Figure 23. Annual profitability results of operating a commercial MightyPOD container in six North American locations measured in USD.

Considering the initial investment of USD 827,384 for the MightyPOD container, the time required to recoup this investment is summarized below in terms of payback periods in Figure 24.

Through the analysis of operating each mining system in each location, it becomes clear that Quebec is the most attractive location to heat greenhouses in as it generates the highest annual profit and lowest payback periods in all settings. This is primarily due to the low domestic electricity rate of USD 0.054/kWh. Similarly, California is the least desirable location to use cryptocurrency miners to heat greenhouses as the operation runs at a deficit, unable to achieve a payback of the initial investment in all settings due to its high electricity rate of 0.29/kWh.

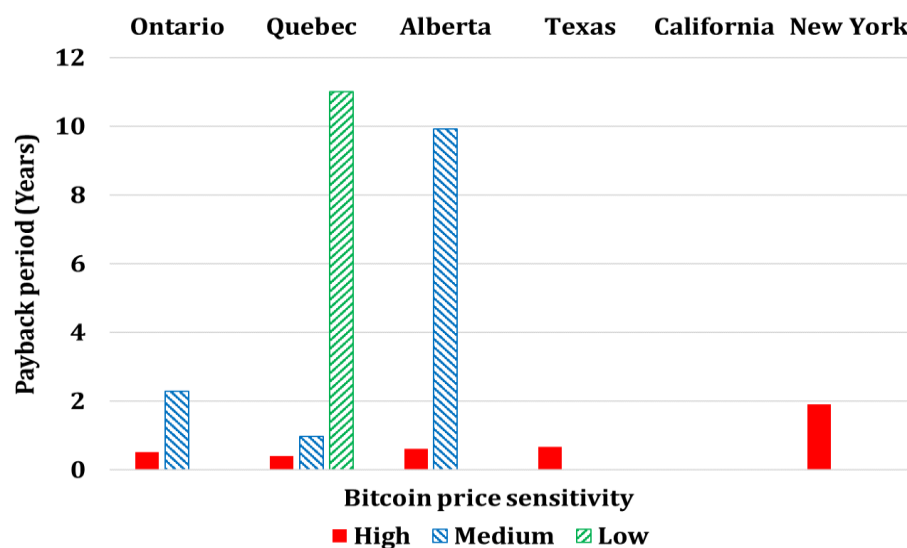


Figure 24. Payback period results from the initial investment for a commercial MightyPOD container operating in six North American locations measured in years.

4.5.2. Natural Gas Heat Source

To analyze the natural gas economic expense requirement to heat comparable greenhouses denoted by Greenhouse 1, Greenhouse 2, and Greenhouse 3, respectively. These greenhouses were analyzed in the six North American locations, where quotes were obtained from natural gas providers in each respective location. For Ontario, Quebec, and Alberta, the natural gas providers Enbridge [71], Energir [72], and Direct Energy Regulated Services (DERS) [73], respectively, were consulted for an estimated annual quote, including ancillary charges to heat each greenhouse volume. Residential quotes were obtained for Greenhouse 1, while commercial quotes were used for Greenhouse 2 and Greenhouse 3. For California, Texas, and New York, the U.S. Energy Information Administration [74] was consulted for both residential and commercial quotes, which included all ancillary charges and taxes. The annual consumption of natural gas required to heat each greenhouse was found to differ depending on geographic location. This is due to differences in the sizes of greenhouses and surrounding environmental factors such as ambient temperature and varying intensities of solar heat unique to each location when running thermal simulations. The annual consumption of natural gas in m³ required for each greenhouse is summarized by location below in Table 5.

Table 5. Annual Natural Gas consumption (m³) for greenhouse heating in six North American locations.

Location	Greenhouse 1 Consumption (m ³)	Greenhouse 2 Consumption (m ³)	Greenhouse 3 Consumption (m ³)
Ontario	598	28,200	222,823
Quebec	571	27,106	217,687
Alberta	677	32,148	254,763
California	546	27,849	226,889
Texas	265	14,239	117,401
New York	614	30,108	243,118

Considering natural gas prices are subject to free market influences of supply and demand, historic monthly natural gas prices in each location were analyzed and averaged over a 12-month period to account for seasonality and rate variability. The annualized natural gas expense in each location for Greenhouse 1 is summarized below in Figure 25.

The annualized natural gas expense in each location for Greenhouse 2 is summarized below in Figure 26.

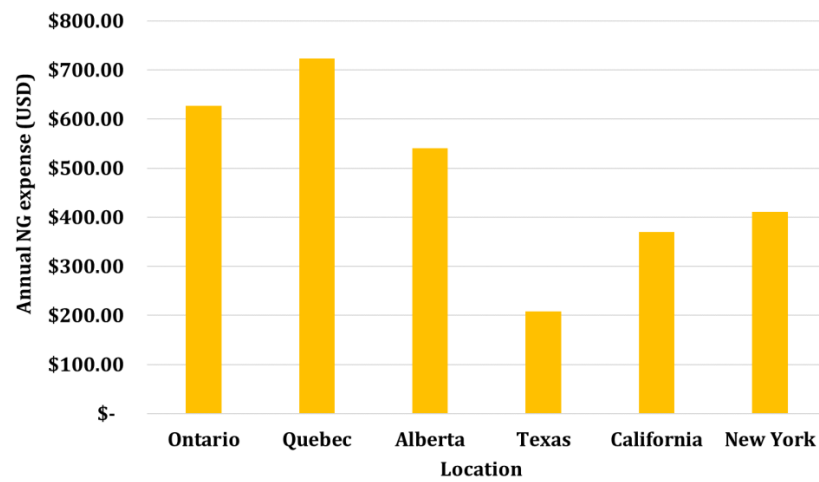


Figure 25. Annual natural gas expense in six North American locations to heat Greenhouse 1.

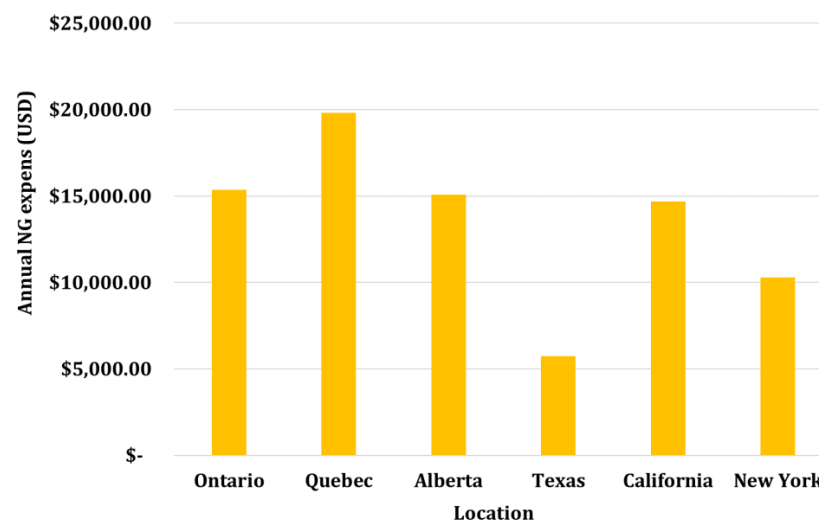


Figure 26. Annual natural gas expense in six North American locations to heat Greenhouse 2.

The annualized natural gas expense in each location for Greenhouse 3 is summarized below in Figure 27.

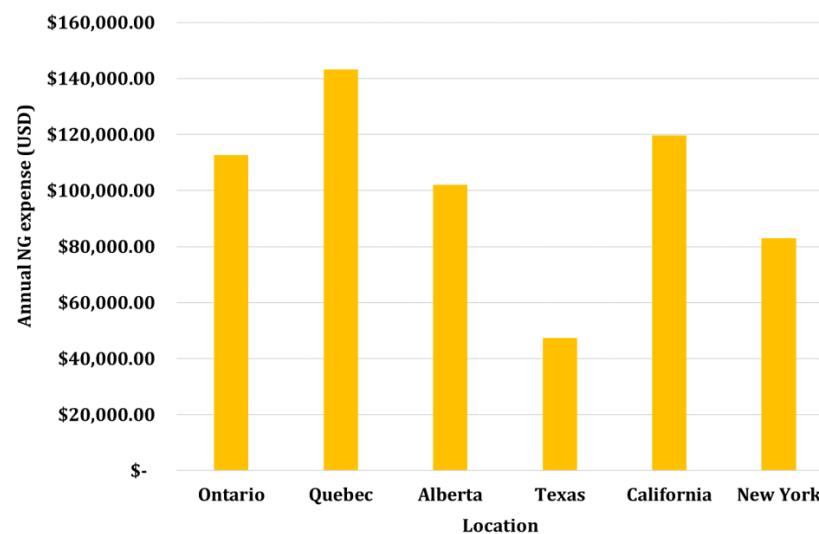


Figure 27. Annual natural gas expense in six North American locations to heat Greenhouse 3.

Through analysis of the annual natural gas expense results, Quebec is the least desirable location to operate a greenhouse utilizing natural gas heating from an economic perspective. This location would incur the highest annual expense for each of the three greenhouse cases. The most desirable location to heat the three greenhouses is Texas, as it incurs the lowest annual expense of all locations. When comparing this annual approach to a granular analysis of each distinct month in Ontario over a one-year period, the results fall within a 1% margin of error. Considering the fluctuations surrounding natural gas rates in the free market and ancillary charges such as delivery fees and load balancing, the annual approach is considered appropriately representative. The monthly natural gas expense analysis for Greenhouse 1 in Ontario is summarized below in Figure 28.

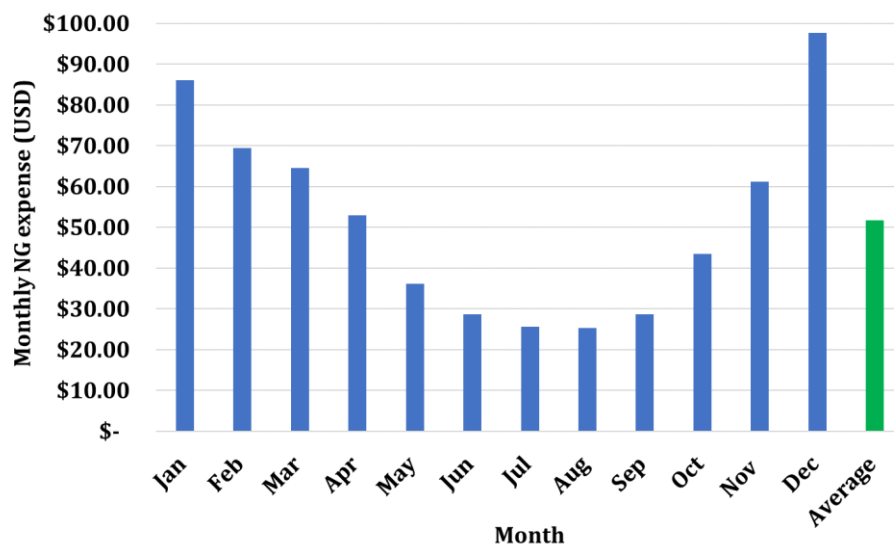


Figure 28. Monthly natural gas expense in Ontario to heat Greenhouse 1.

The monthly natural gas expense analysis for Greenhouse 2 in Ontario is summarized in Figure 29.

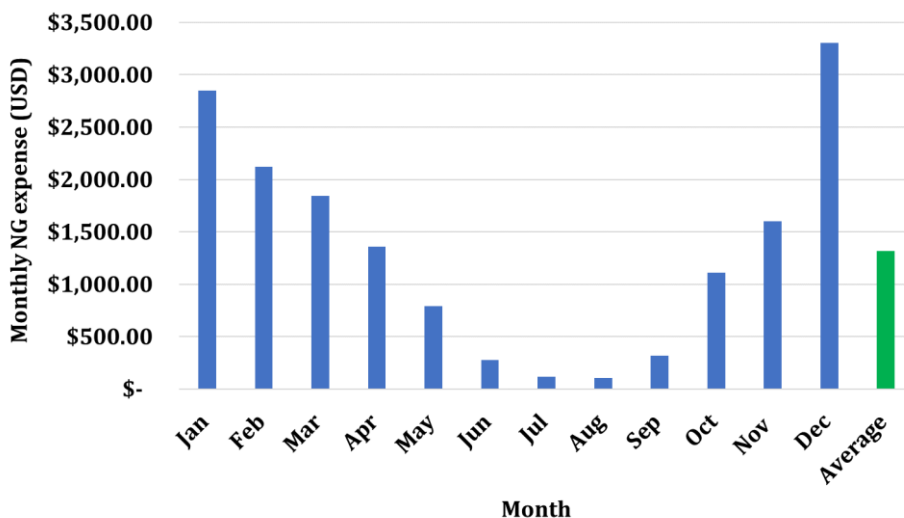


Figure 29. Monthly natural gas expense in Ontario to heat Greenhouse 2.

The monthly natural gas expense analysis for Greenhouse 3 in Ontario is summarized in Figure 30.

The granular monthly analysis of natural gas expenses in Ontario reveals significant fluctuation each month. It is evident that the Canadian winter months of January, February, and December see the highest heating expense of USD 21,038, USD 15,451, and USD

24,519, respectively, compared to the average USD 9066 for Greenhouse 3. This is due to increased heating demand from the cold environment. Similarly, the summer months of June, July, and August see the lowest heating expense of USD 1527, USD 341, and USD 241, respectively, compared to the average of USD 9066. This is the result of a decreased heating demand during these summer months. From a monthly analysis, the monthly heating expense is cyclical based on the seasons and external climate that conforms to a predictable average when taken as a 12-month aggregate. This gives credence to an annualized analysis of natural gas rates for comparison.

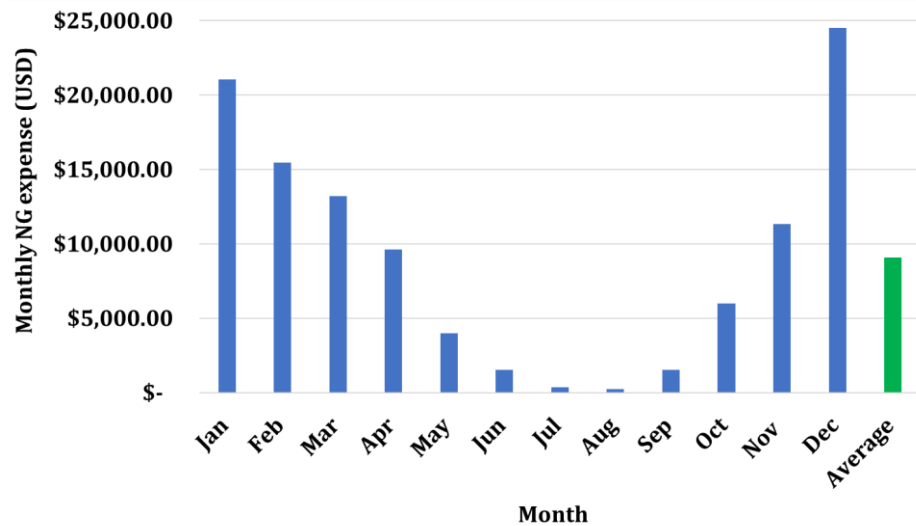


Figure 30. Monthly natural gas expense in Ontario to heat Greenhouse 3.

4.5.3. Natural Gas Expense Compared to Bitcoin Mining Electricity Expense

Comparison between the operating electricity expense of Bitcoin mining for each system and the natural gas expense to heat the three discussed greenhouses enable a thorough understanding of the operating cashflows associated with each heat source. Electricity expense compared to natural gas expense in six distinct locations for Greenhouse 1 is summarized below in Figure 31.

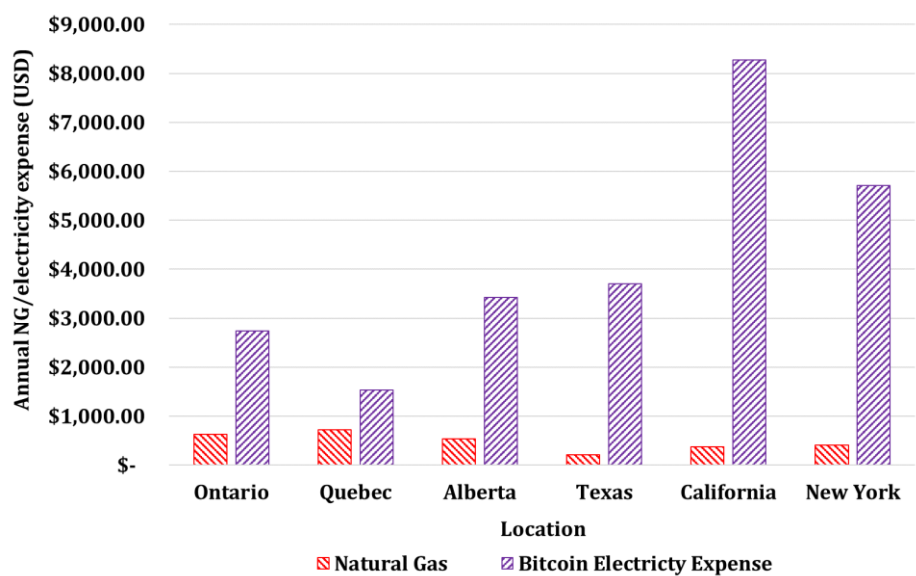


Figure 31. Annual heating expense of natural gas compared to electricity used to operate a Bitcoin mining system in six North American locations to heat Greenhouse 1.

Electricity expense compared to natural gas expense in six distinct locations for Greenhouse 2 is summarized in Figure 32.

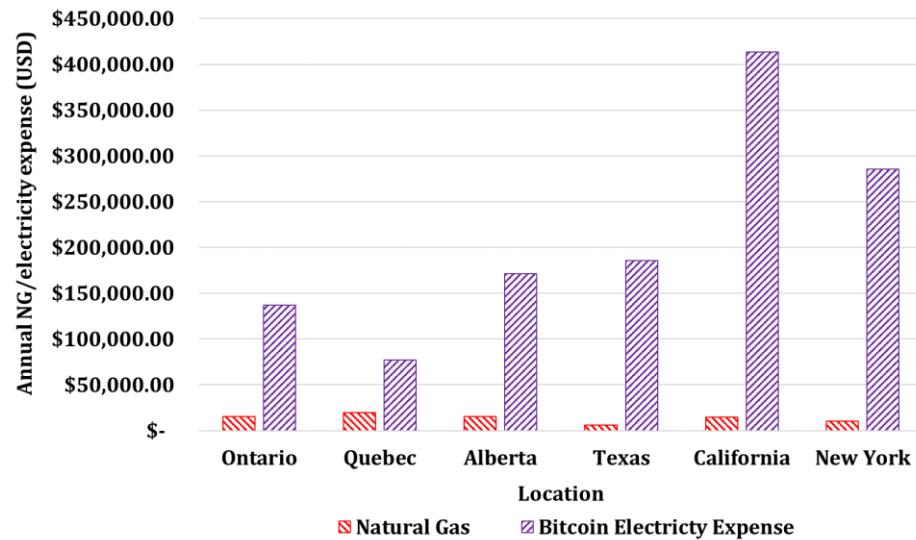


Figure 32. Annual heating expense of natural gas compared to electricity used to operate a Bitcoin mining system in six North American locations to heat Greenhouse 2.

Electricity expense compared to natural gas expense in six distinct locations for Greenhouse 3 is summarized in Figure 33.

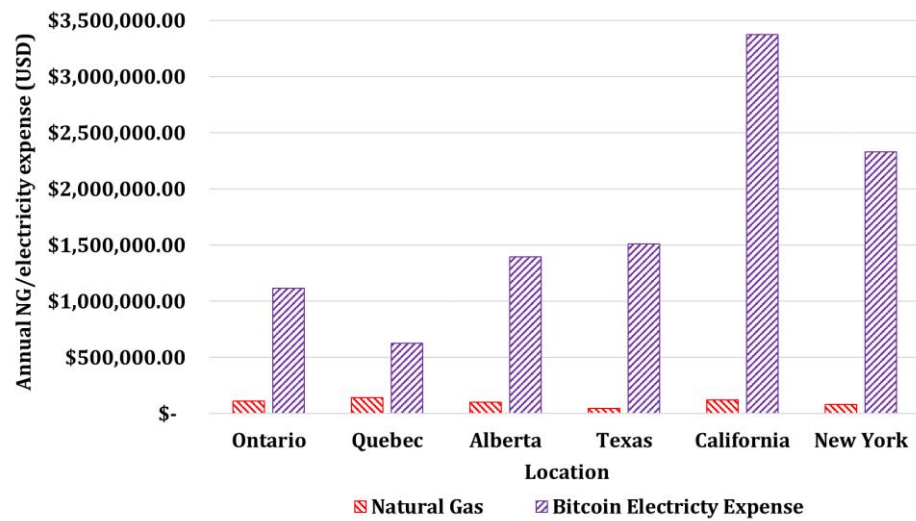


Figure 33. Annual heating expense of natural gas compared to electricity used to operate Bitcoin mining sources in six North American locations to heat Greenhouse 3.

Through comparative analysis of each heat source in each location, it becomes clear that the electricity expense to power the Bitcoin mining systems exceeds the natural gas expense in all scenarios. This is most evident in California when comparing Greenhouse 3. The annual electricity expense is USD 3,375,433 to heat the greenhouse with the appropriate Bitcoin mining system compared to USD 119,580 for heat with natural gas. However, depending on geographic location and the domestic electricity rates, this difference is significantly decreased. In Quebec, the annual electricity expense is USD 628,529 to heat the same greenhouse with a Bitcoin mining system compared to an annual natural gas heating expense of USD 143,154. This represents a 339% increase in additional operating expenses to use Bitcoin mining systems compared to the 2723% increase in operating expenses found in

California, which highlights the importance of location. This analysis provides greenhouse operators insight into the operating expenses required for each heating source to plan their cashflows accordingly. It is important to note that these annual electricity expenses do not account for the offset in revenue generated from the production of Bitcoin during the mining process.

4.5.4. Heat Source Comparison

Economic analysis of greenhouse heating utilizing either Bitcoin mining systems or natural gas can have a significant impact on the net profitability of a greenhouse farmer. Annual heating expense comparison between the two heat sources after accounting for the sale of produced Bitcoin for Greenhouse 1 is summarized below in Figure 34. Negative values indicate an operational profit for the Bitcoin mining systems after selling the produced Bitcoins and paying their electrical operating expense.

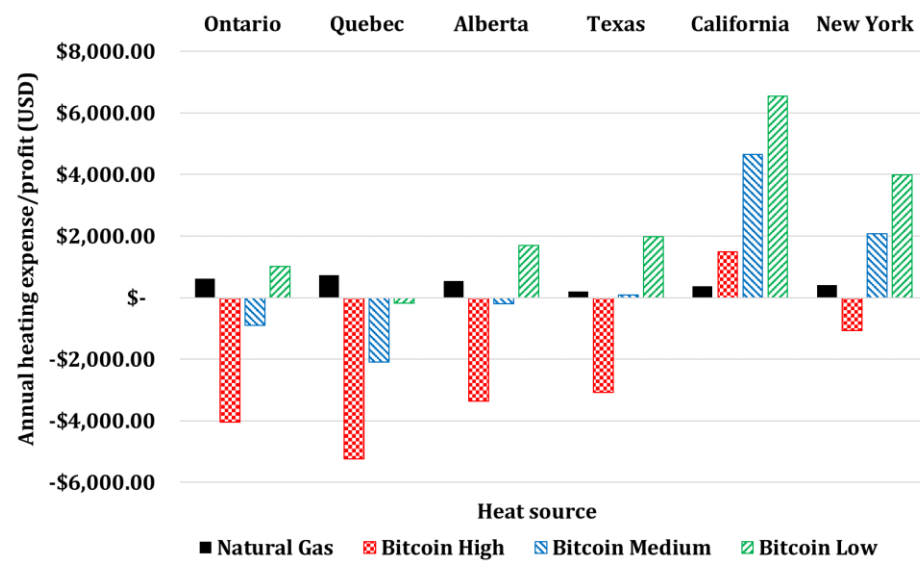


Figure 34. Annual heating expense/profit with natural gas and Bitcoin mining (after considering Bitcoin selling price) sources in six North American locations to heat Greenhouse 1.

The annual heating expense comparison between the two heat sources for Greenhouse 2 is summarized below in Figure 35.

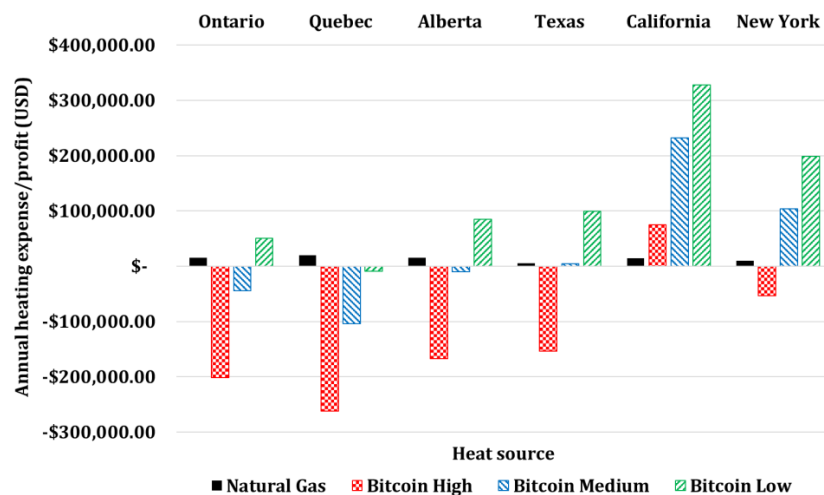


Figure 35. Annual heating expense/profit with natural gas and Bitcoin mining (after considering Bitcoin selling price) sources in six North American locations to heat Greenhouse 2.

The annual heating expense comparison between the two heat sources for Greenhouse 3 is summarized below in Figure 36.

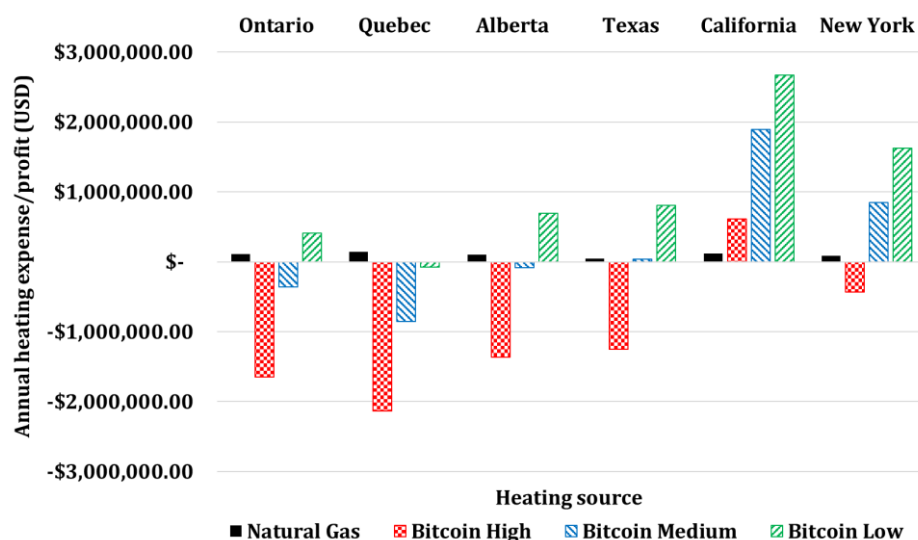


Figure 36. Annual heating expense/profit by natural gas and Bitcoin mining (after considering Bitcoin selling price) sources in six North American locations to heat Greenhouse 3.

Economic comparison when factoring in the sale of Bitcoin reveals that greenhouse heating with a Bitcoin mining heat source has the potential to convert a consistent operating expense, as seen with natural gas heating, into a lucrative alternative revenue stream. Quebec experiences the most dramatic profitability change when converting between the two heating sources, as seen with Greenhouse 3. Natural gas heating would cost an operator USD143,154 annually to heat this greenhouse. However, with a Bitcoin mining heat source, an operator has the potential to convert this expense into an annual net profit of USD 2,135,925 in the high Bitcoin price sensitivity after paying the operating electrical expense. In the low Bitcoin price sensitivity case, an operator in Quebec can expect a USD 75,190 annual net profit. However, for the same greenhouse in California, where the electricity rates are higher, Bitcoin mining as a greenhouse heat source has the potential to incur a greater expense than natural gas. Annual natural gas expense in California for this greenhouse would be USD 119,581 compared to the Bitcoin mining heat source annual electrical expenses of USD 610,979, USD 1,895,345, and USD 2,671,714 in the high, medium, and low Bitcoin price sensitivity cases, respectively. This demonstrates the potential economic incentives and liabilities when leveraging Bitcoin mining systems as a heat source which are contingent on the price of Bitcoin and geographic location.

5. Discussion

5.1. Heating with Miners in Practice

Potential business opportunities exist for the application of Bitcoin mining systems to heat greenhouses. The nature of these opportunities differs depending on the owner/operator of the Bitcoin mining systems. Based on prior analysis, the application of Bitcoin mining systems is ideal in locations where electricity rates are lowest and during prosperous economic conditions for the Bitcoin valuation. The first opportunity exists for greenhouse farmers who own and operate Bitcoin mining systems to heat their greenhouses for crop production. These farmers will obtain the potential to convert a traditional fixed expense of natural gas heating into a profitable process to supplement crop production. This can be achieved by replacing natural gas heating with a comparable Bitcoin mining system and incurring the initial investment. Greenhouse farmers will utilize the generated Bitcoin to pay the electrical expense of the system and recoup the initial investment. Excess Bitcoin will be treated as profit while the mining system exhausts heat for the greenhouse.

The second opportunity exists for contractors leveraging the Bitcoin mining system's exhaust heat to provide to greenhouse farmers as a service. This service could be provided to any greenhouse farmer capable of supplying appropriate power to the Bitcoin mining system. Contractors are capable of charging greenhouse farmers a fee equivalent to or, more likely, less than their existing natural gas expense bill to incentivize them to use the service. Contractors would be responsible for paying the electricity expense of the Bitcoin mining system, which can be done using Bitcoins produced through the process. Contractors would look to prioritize locations with the lowest domestic electricity rates and the highest natural gas rates to maximize the threshold of their service charge and optimize profit margins. It is important to note that the transportation costs associated with delivering the necessary hardware for the heating service would vary depending on the location of the heating source to its destination. These costs would be highly variable depending on the type of carrier vehicle required for delivery. Traditional transportation means will be able to transport the individual Antminer S17e, while industrial trailers will be needed to tow the commercial mining systems. In general, these systems would be stationary for a long period but could be mobile in the event of electricity rate changes, carbon emission incentives, or other policy changes.

Lastly, a symbiotic relationship between Bitcoin mining operators and greenhouse farmers can be established to improve profitability for each party involved. This is achieved by Bitcoin mining operators paying farmers for electricity at a reduced rate to the domestic rate in exchange for the exhaust heat from the Bitcoin mining system. This will decrease the operating expense for Bitcoin mining operators through the compromise on the heat byproduct that is traditionally discarded. Farmers will be able to supplement their heating efforts to grow crops and reduce their expenditures on natural gas heating to improve profitability as a result. This operation would be most likely for farms deploying agrivoltaic systems (dual use of land for agriculture and solar photovoltaic electricity generation) and thus possessing large quantities of low-cost renewable electricity (details discussed in Section 5.3).

5.2. Limitations of Study

Three sizes of greenhouses (domestic, semi-commercial, and commercial) have been introduced for tomato cultivation exploiting the waste heat of cryptocurrency miners under three miner orientation scenarios (individual Antminer S17e miner, DIY Mining Container with 50 miners, and MightyPOD Commercial Mining Container with 408 miners). The mathematical quasi-steady state model was developed for the simulation of the thermal performances of the greenhouses on an hourly basis. The sizes of greenhouses have been calculated considering their maximum heating demands on the coldest day of the year. It is expected to implement a transient model for the thermal performance of the greenhouse [75–77] in order to enable the introduction of an adaptive heating supply system and utilization of the excess waste heat of miners for other useful purposes. Maintaining the inside temperature of the greenhouse at a fixed value is not achievable in practice, even though it is highly required for conducting the technical feasibility analysis of a sustainable heating supply system for greenhouse applications. This work aimed at conducting such studies to come up with the idea of reducing the dependency of greenhouses on the natural gas grid.

Growing other vegetables such as cucumber and pepper, the principal greenhouse vegetable crops with a relatively dominant economic contribution in the horticultural sector in Canada [78], is highly required to be investigated in net-zero or near-zero energy greenhouses heated by the waste heat of data centers or mining farms. To simplify the proposed technical model and avoid providing excess content, the techno-economic feasibility of the above-mentioned idea has been assessed merely for tomato cultivation in Canadian greenhouses.

The acquired natural gas quote's associated ancillary fees, such as distribution, transportation, and load balancing, make up a significant portion of what can be expected on a

monthly natural gas heating bill. The values given represent generalized approximations in each location that are subject to change depending on where, specifically, the greenhouse operation is located within each analyzed province or state. Depending on this location, accessibility to this study's quoted providers may not be possible, thus altering the expected natural gas expenditures if pursued. Natural gas rates are also influenced by rate class, utility zoning, and infrastructure implementation to receive the service. These values are incorporated as generalized approximations that may vary depending on location and alternative providers. Natural gas is traded on North American markets allowing for the 12-month average rates used in this study to be subject to significant change. Weather and geopolitical factors, such as the Russia and Ukraine war, have also impacted recent quotation estimates used within this study that may not be representative of standard natural gas price conditions. Russia is a major supplier to North America that cannot conduct trade due to sanctions imposed on them from their war with Ukraine [79]. This has decreased the available supply of oil and natural gas while demand remains the same in the economy, causing a premium charge to be placed on the product. It is not feasible to assume a constant production of 0.098 Bitcoin for each Antminer S17e in perpetuity, as done in this study. There are several factors that influence the production of Bitcoin by a miner, such as network difficulty, which increases as more people participate in mining, effectively reducing the production by the existing miners. As better hardware is innovated that increases hashing capabilities, older models such as the Antminer S17e will produce less Bitcoin annually as network difficulty increases, reducing its profitability.

Current global economic conditions should be considered by any operator looking to utilize Bitcoin mining as a heat source due to the importance that Bitcoin's price has on the profitability of an operation. The United States inflation rate was reported at 7.1% in October 2022, which has fallen from 9.1% in August 2022 [80]. The Federal Reserve has a 2% target inflation rate and is committed to regularly increasing interest rates until that goal is met [81]. With the current Federal Reserve interest rate at approximately 4% with forecasted 0.75% raises [82], all major indices and cryptocurrencies have experienced a recent decline in value as investors de-risk [83]. In this economic climate, Bitcoin's price may continue to decline toward prices not contained by the low-case sensitivity adjustment used in this study. This will lead to a more expensive heating source than natural gas and longer payback periods of the initial investment in certain locations.

5.3. Future Work to Couple with Photovoltaics

Previous work [62] has shown that solar photovoltaic (PV) systems can be used for powering cryptocurrency farms profitably. Future work should consider coupling field agrivoltaics [84] with greenhouse-integrated PV [85–87] to provide the electricity to heat the greenhouses with heat pumps, cryptocurrency miners, and other types of computing and servers. As Ontario considers agrivoltaics [88], such integration has been demonstrated in Ontario greenhouses with partially-transparent PV modules [89,90]. Substantially more research is needed to optimize greenhouse PV modules in specific planting systems [91] by investigating density, type of module (e.g., thin film or wafer-cell-based) size, as well as the chemical composition of nanoparticles that perform spectral shifting via fluorescence [92–94]).

6. Conclusions

A novel greenhouse thermal model was developed and validated. The thermal model was used to perform sensitivity studies on three greenhouse sizes for three computing facilities in six locations in North America. First, the effect of air exchange rate variations showed that the variation in the size of the residential greenhouse is almost 2.5% and is about 7–7.5% of the commercial greenhouses. Increasing the lighting allowance factor caused an increase in greenhouse sizes. Nevertheless, the heating demand of all three greenhouses tended to decrease since the impact of the increment of the heat dissipation through the lighting system was more notable than the enlargement of the greenhouses.

Changing the photoperiod of the crops from 14 to 20 h per day led to an increasing–decreasing trend in greenhouse sizes. Raising the photoperiod leads to a reduction in the number of lights that should be used, which in turn causes an increase in the accumulative thermal energy absorbed by the greenhouses. The photoperiod of 17–19 h per day provides the maximum greenhouse sizes for all miner scenarios. Finally, increasing the planting area fraction from 0.6 to 0.9 naturally increased the contribution of evapotranspiration heat loss in the greenhouses, thereby reducing the greenhouse sizes and cooling demands while increasing their heating requirements.

Through the conversion of a natural gas greenhouse heating source to a Bitcoin mining heating source, a greenhouse operator has the potential to convert a fundamental expense of their operation into a profitable alternative revenue stream. This is most clearly seen in Quebec, where natural gas heating expenditures are the highest and electricity rates to power Bitcoin miners are the lowest. The magnitude of change is significant in all greenhouse sizes analyzed and most apparent with Greenhouse 3 due to increased scale. The annual natural gas heating expense in Quebec for this greenhouse would be USD143,154 in comparison to the Bitcoin mining heat source converting the heating expense into an annual net profit of USD 2,135,925 in the high case Bitcoin price sensitivity. The profitability of the Bitcoin mining heat source is contingent on the price of Bitcoin and the price of electricity in the area. These variables significantly influence the results, as seen with the low-case Bitcoin price sensitivity in the same location yielding a USD75,190 annual net profit. Given this variability, operators are exposed to increased financial risk and uncertainty as the price of Bitcoin unpredictably fluctuates. Deciding where to operate a greenhouse is a critical component for operational efficiency, regardless of the heat source used. When analyzing Greenhouse 3, the annual natural gas expense varies significantly between the cheapest location, Texas, at USD 47,375, to the most expensive, Quebec, at USD 143,154. This represents approximately a 202% increase in expenditures on the basis of location. When utilizing a Bitcoin mining heat source with a medium Bitcoin price sensitivity of USD 37,017 in Quebec, an operator yields USD 851,558 in annual profit. Under the same conditions, if an operator chose to operate in California, they would experience a USD 1,895,345 annual expense making the process unprofitable compared to a consistent natural gas expense of USD 82,960.

Using the methods provided in this study, appropriate locations for mining waste heat reclamation for greenhouses can be determined. There are many factors influencing the feasibility of Bitcoin mining to heat greenhouses, as mentioned, with location (weather and utility rates) and the price of Bitcoin. Thoughtful accommodation for these variables by greenhouse operators and Bitcoin heating service providers has the potential to create a lucrative heating process. This can be achieved through the transition of the traditional heating expense of natural gas and the associated greenhouse gas emissions into profitable heating using electrification (and the potential of reduced emissions with renewable energy generation) through the process yielding Bitcoin or other types of cryptocurrency.

Author Contributions: Conceptualization, J.M.P.; methodology, N.A. and M.T.M.; software, N.A.; validation, N.A. and M.T.M.; formal analysis, N.A. and M.T.M.; investigation, N.A. and M.T.M.; resources, J.M.P.; data curation, N.A. and M.T.M.; writing—original draft preparation, N.A., M.T.M. and J.M.P.; writing—review and editing, N.A., M.T.M. and J.M.P.; visualization, N.A., M.T.M.; supervision, J.M.P.; project administration, J.M.P.; funding acquisition, J.M.P. All authors have read and agreed to the published version of the manuscript.

Funding: This work was supported by the Thompson Endowment, the Western University Carbon Solutions program, and the Natural Sciences and Engineering Research Council of Canada.

Data Availability Statement: The code is available under GNU GPL v3 on the Open Science Framework [95].

Conflicts of Interest: The authors declare no conflict of interest.

Appendix A. (Greenhouse Theoretical Calculations)

All the mathematical equations and necessary assumptions for the required parameters are provided here. MATLAB software has been used for simulation, and the code is available under GNU GPL v3 on the Open Science Framework [95].

Appendix A.1. Solar Radiation

The heat gained from the solar radiation equals the available solar radiation multiplied by the area and the transmissivity of the greenhouse cover [8]:

$$Q_{solar} = \sum \tau_i A_i I_i, \quad (A1)$$

here, τ_i and A_i represent the solar transmissivity of the greenhouse cover and area of the i th surface in (m^2), respectively. I_i is the hourly solar radiation on the sloped surfaces in (J/m^2) and can be calculated using the isotropic sky model [96]:

$$I_i = I_b \frac{\cos\theta_i}{\cos\theta_z} + I_d \left(\frac{1 + \cos\beta}{2} \right) + (I_b + I_d) \rho_g \left(\frac{1 - \cos\beta}{2} \right), \quad (A2)$$

in which “ b ” and “ d ” indices correspond to the beam and diffuse radiation, respectively. ρ_g is the ground reflectance, which is usually provided for different months [96]. β , θ_i , and θ_z are the angle of sloped surfaces, the angle of incidence of beam radiation, and the zenith angle, respectively [96]. SAM (System Advisor Model) free software of NREL (National Renewable Energy Laboratory) has been used in order to calculate the hourly solar radiation on tilted surfaces of the greenhouse.

The physical characteristics of covering materials are presented in Table A1:

Table A1. Physical characteristics of greenhouse covering materials.

Physical Characteristic	Value	Reference
Tempered glass		
Transmissivity (τ_G)	0.88–0.93	[97]
Transmissivity to long-wave radiation ($\tau_{G,l}$)	0.03	[97]
Emissivity (ε_G)	0.88–0.9	[96,97]
Thermal conductivity (k_G)	0.76 W/mK	[97]
Twinwall polycarbonate		
Transmissivity (τ_{PC})	0.78–0.82	[8,54,97,98]
Transmissivity to long-wave radiation ($\tau_{PC,l}$)	0.03	[8,97]
Emissivity (ε_{PC})	0.65–0.89	[8,54,97]
Thermal conductivity (k_{PC})	0.17–0.2 W/mK	[8,54,97]

Appendix A.2. Supplementary Lighting

One of the most significant objectives of supplementary lighting is to increase the photosynthesis of plants. The required amount and the operating time of supplementary lighting are deducible from the optimum daily light integral (DLI) required for plant growth. The optimum value of DLI for tomatoes is $25 \text{ mol}/m^2\text{day}$ [53,99]. In London, the average DLI provided by the sun can be found in Ref. [100]. Its hourly value can also be calculated by Equation (A3) and using available hourly solar irradiation [99]:

$$DLI_{sun} = 2.15 \times 10^{-6} \frac{\sum \tau_i A_i I_i}{A_{gh}} \quad (A3)$$

The remaining required DLI (DLI_{light}) must be met by the supplementary lighting system. Depending on the type of lamps, the supplementary lighting system can return about 60–100% of the consumed energy as heat to the greenhouses [8,45,99]. It is assumed that the supplementary lighting system is composed of LED (light-emitting diode) lamps. LEDs have some advantages (high efficiency, longer lifespan, and their capability to control spectral composition) over conventional lighting fixtures [101]. Having the DLI_{light} in

hand, the actual electricity consumption rate of LED lamps in (W/m^2) can be derived using Equation (A4):

$$\dot{W}_{LED} = \frac{DLI_{light} \times 10^6}{F_{lc} n_{light} \times 3600} F_a, \quad (\text{A4})$$

in which, n_{light} is the maximum allowable hours of supplementary lighting to prevent plants from chlorosis. In general, the maximum day length (photoperiod) for fruiting vegetables (e.g., tomatoes, cucumbers, and peppers) should be between 14–20 h/day [53,99]. This period can be considered for tomatoes in both vegetative and fruiting/flowering stages 16 h/day [45,99]. It is also worth mentioning that supplementary lighting can be performed in the early morning and late afternoon [102]. In Equation (A4), F_{lc} stands for the light conversion coefficient that can be considered $3.5 \mu\text{mol}/\text{J}$ for modern LEDs [99]. F_a is the lighting allowance factor, the ratio of the lighting fixtures' power consumption to their nominal power consumption, which is considered to be 0.9–1.1 for high-wattage lamps [103].

The thermal waste heat dissipated from the lamps in (J) can be obtained from the equation below [8]:

$$Q_{light} = W_{LED} F_{hc} A_{gh}, \quad (\text{A5})$$

here, F_{hc} is the heat conversion factor, the amount of energy converted to radiative thermal energy, which can be derived from $(1 - \eta_{light})$ [102]. η_{light} can be assumed to be 0.4 for LEDs [99].

Appendix A.3. Conduction and Convection Heat Loss through the Walls

The conductive and convective heat losses through the greenhouse walls and roof can be calculated via Equations (A6) and (A7) [8]:

$$Q_{cc} = (T_i - T_o) \sum U_i A_i, \quad (\text{A6})$$

$$U_i = \left[\frac{1}{h_i} + \frac{\delta_G}{k_G} + \frac{\delta_{PC}}{k_{PC}} + \frac{1}{h_a} + \frac{1}{h_o} \right]^{-1}, \quad (\text{A7})$$

T_i and T_o are the inside and the outside temperatures in (K), respectively. U_i is the overall heat transfer coefficient of each surface in ($\text{W}/\text{m}^2\text{K}$). δ and k are the thickness in (m) and the thermal conductivity of the cover in (W/mK), respectively. h_a is the heat transfer coefficient of insulation air in double-layered walls, which is usually assumed to be $3.85 \text{ W}/\text{m}^2\text{K}$ [8]. The value of $\left(\frac{\delta_{PC}}{k_{PC}} + \frac{1}{h_a} \right)^{-1}$ is provided for commercial polycarbonate covers [98]. The inside air velocity is near zero (0.2 m/s [8,45]), and consequently, it can be assumed that its heat transfer phenomenon is free convection. So, h_i , convective heat transfer coefficient between the inside air and the greenhouse cover, can be estimated using Equation (A8) [8].

$$h_i = \frac{k_a}{L_c} 0.1 (GrPr)^{0.33}, \quad \text{for } 10^9 \leq GrPr \leq 10^{13} \quad (\text{A8})$$

$$Gr = \frac{g \beta_a (T_i - T_c) L_c^3}{\left(\frac{\mu_a}{\rho_a} \right)^2}, \quad (\text{A9})$$

$$Pr = \frac{\mu_a C p_a}{k_a} \quad (\text{A10})$$

In the above equations, L_c is the characteristic length of the related surface, and g corresponds to the gravity of the Earth with the value of 9.81 m/s^2 . $C p_a$, k_a , μ_a , and β_a are the air heat capacity in (J/kgK), the air thermal conductivity, the viscosity of film on the surfaces in (kg/sm), and the volumetric expansion coefficient of air in ($1/\text{K}$), respectively. All these values can be calculated in T_{film} , which can be estimated using Equation (A11) [104]. Also, T_c stands for the cover temperature, which can be estimated using Equation (A12) [52]:

$$T_{film} = \frac{T_c + T_i}{2}, \quad (\text{A11})$$

$$T_c = \frac{2}{3}T_o + \frac{1}{3}T_i \quad (\text{A12})$$

h_o , the convective heat transfer coefficient between the outside air and the greenhouse cover can be calculated for the turbulent flows by the equation below [8,104]:

$$h_o = \frac{k_a}{L_c} 0.037 Re^{0.8} Pr^{0.33}, \quad \text{for } Re \geq 5 \times 10^5 \quad (\text{A13})$$

$$Re = \frac{\rho_a v_\infty L_c}{\mu_a}, \quad (\text{A14})$$

where, v_∞ represents the wind speed in (m/s).

Appendix A.4. Heat Loss through the Air Exchange

Air exchange between the greenhouse and the outdoors is caused by infiltration and ventilation. The minimum level of infiltration rate has been reported as 0.2–0.5 ACH (h^{-1}) in references [105,106]. Since the CO_2 concentration in the atmosphere can cover the minimum level of tomato plants' requirement for photosynthesis (360–400 ppm of CO_2) [45], the natural ventilation would be considered only for the summer with the aim of maintaining the inside temperature and relative humidity in a desirable level [8,107]. Even for the winter, however, the minimum level of 0.7–1 ACH total air exchange can be maintained for the greenhouses without supplementary CO_2 supply systems and with a constant relative humidity of above 80% [8,107,108]. Therefore, the heat loss through the air exchange can be calculated using Equation (A15) [5,58]:

$$Q_{airex} = Q_{inf} + Q_{vent} = \dot{V}_a \rho_a C p_a (T_i - T_o) \cong 0.33 N_v V_g (T_i - T_o), \quad (\text{A15})$$

where, V_g is the greenhouse volume in (m^3) and N_v is the number of natural air exchanges per hour.

Appendix A.5. Heat Loss through the Long-Wave Radiation

The hourly long-wave radiation from the greenhouse ground and plants (Q_{lwr}), which is transmitted to the sky or absorbed by the cover, can be expressed as follows [8]:

$$Q_{lwr} = \left[\sigma \varepsilon_p (T_i^4 - T_c^4) F_{p-c} A_f \right] + \left[\sigma \varepsilon_p \tau_c F_{p-sky} A_f (T_i^4 - T_{sky}^4) \right] \quad (\text{A16})$$

The first term on the right side of the equilibrium can be rewritten from the greenhouse cover perspective:

$$\sigma \varepsilon_p (T_i^4 - T_c^4) F_{p-c} A_f = \sigma (T_i^4 - T_c^4) \sum \varepsilon_c F_{c-p} A_c \quad (\text{A17})$$

In Equations (A16) and (A17), subscripts "c" and "p" are attributed to the cover and plants of the greenhouse, respectively. σ is the Stephan–Boltzmann constant ($5.67 \times 10^{-8} \text{ W/m}^2\text{K}^4$), and ε and τ represent the emissivity and long-wave transmissivity of the related surfaces. The emissivity of ground and plants is considered 0.9 [8]. F_{p-sky} is the view factor between the greenhouse and the sky, which equals 1, and F_{c-p} stands for the view factor between the plants on the floor and the covers, which can be calculated by the equation below [8]:

$$F_{c-p} = \frac{1 + \cos\theta}{2} \quad (\text{A18})$$

T_{sky} can be estimated as follows [109]:

$$T_{sky} = 0.055 T_o^{1.5} \quad (\text{A19})$$

A thermal curtain can be used at night to reduce the longwave radiation through the greenhouse roof [110].

Appendix A.6. Heat Loss through the Greenhouse Floor

The heat losses through the greenhouse floor are related to the thermal losses from the soil to the deep ground [8,109]:

$$Q_{floor} = \frac{k_s}{H_s} A_f (T_f - T_g) T_{sky} = 0.055 T_o^{1.5}, \quad (A20)$$

where k_s is the thermal conductivity of the soil, which is assumed to be 1.25–1.4 W/mK [8,111]. Moreover, T_g is the deep ground temperature, which varies between 6 to 11 °C during the year [50], and H_s the maximum depth of soil, where the temperature gradient tends to the minimum level. It is a reasonable assumption to take the floor temperature (T_f) equal to the greenhouse temperature.

Appendix A.7. Heat Loss through the Evapotranspiration

Evapotranspiration represents the water evaporated from the floor and transpired by plants. Since the modeling of evaporation from the floor is complicated, it is a rational assumption to consider it to be included in the evapotranspiration from the plants' surfaces (i.e., leaves) [8]. The amount of heat used for the evapotranspiration of plants can be affected by different factors (e.g., solar radiation, air humidity, wind), which can be estimated as follows [8,45]:

$$\dot{Q}_{evap} = \dot{m}_{mois} h_v, \quad (A21)$$

where h_v is the latent water heat of vaporization in (J/kg). The excess thermal energy inside of the greenhouse leads to the plants' transpiration, whose mass flow rate (\dot{m}_{mois}) can be calculated by the equation below in (kg/s) [112]:

$$\dot{m}_{mois} = A_p \rho_a \frac{\omega_{ps} - \omega_i}{R_a + R_s} \quad (A22)$$

A_p is the actual surface area of all the plant leaves in (m²). This parameter can be estimated using the average leaf area index of the plant (LAI), which is 2.0 m²/m² for tomatoes [8], multiplied by the actual area on the greenhouse floor dedicated to planting. ω_{ps} and ω_i define the saturated humidity ratio of plant surface and indoor air of the greenhouse, respectively, and can be calculated using the following equations [8]:

$$\omega_{ps} = 0.622 \frac{P_g}{P_a - P_g}, \quad (A23)$$

$$\omega_i = 0.622 \frac{\phi_i P_g}{P_a - \phi_i P_g}, \quad (A24)$$

where P_a and P_g stand for the indoor pressure and saturated pressure in indoor temperature, respectively. Additionally, ϕ_i corresponds to the relative humidity of indoor air in the greenhouse.

Finally, the aerodynamic resistance (R_a) and the stomatal resistance (R_s) with the unit (s/m) can be estimated from the following relationships [113]:

$$R_a = 220 \frac{L_{leaf}^{0.2}}{v_i^{0.8}}, \quad (A25)$$

$$R_s = 200 \left(1 + \frac{1}{e^{(0.05(\tau I_g - 50))}} \right) \quad (A26)$$

L_{leaf} represents the characteristic length of plant leaves (0.027 m for tomatoes) [8], and v_i is the indoor air velocity. I_g is the hourly global solar radiation on the horizontal surface in (W/m²). The transpiration of the vast majority of plants tends to occur during daylight hours, and this process reaches its maximum level at noon [45,56]. Therefore, it is a reasonable assumption to consider the evapotranspiration heat losses from sunrise to sunset.

References

1. Gorjian, S.; Calise, F.; Kant, K.; Ahamed, M.S.; Copertaro, B.; Najafi, G.; Zhang, X.; Aghaei, M.; Shamshiri, R.R. A Review on Opportunities for Implementation of Solar Energy Technologies in Agricultural Greenhouses. *J. Clean. Prod.* **2021**, *285*, 124807. [[CrossRef](#)]
2. The United Nations Department of Economic and Social Affairs. *The Sustainable Development Goals Report*; The United Nations Department of Economic and Social Affairs: New York City, NY, USA, 2022.
3. FAO. *Early Warning Early Action Report on Food Security and Agriculture*; FAO: Rome, Italy, 2019.
4. Fox, J.A.; Adriaanse, P.; Stacey, N.T. Greenhouse Energy Management: The Thermal Interaction of Greenhouses with the Ground. *J. Clean. Prod.* **2019**, *235*, 288–296. [[CrossRef](#)]
5. van Straten, G.; van Willigenburg, G.; van Henten, E.; van Ooteghem, R. *Optimal Control of Greenhouse Cultivation*; Taylor and Francis Group, LLC: Abingdon, UK, 2011; ISBN 978-1-4200-5961-8.
6. Altes-Buch, Q.; Quoilin, S.; Lemort, V. A Modeling Framework for the Integration of Electrical and Thermal Energy Systems in Greenhouses. *Build. Simul.* **2022**, *15*, 779–797. [[CrossRef](#)]
7. Crops and Horticulture Division, Agriculture and Agri-Food Canada. *Statistical Overview of the Canadian Greenhouse Vegetable Industry*; Government of Canada Publications: Ottawa, ON, Canada, 2020.
8. Ahamed, M.S.; Guo, H.; Tanino, K. A Quasi-Steady State Model for Predicting the Heating Requirements of Conventional Greenhouses in Cold Regions. *Inf. Process. Agric.* **2018**, *5*, 33–46. [[CrossRef](#)]
9. Yarosh, M.M.; Nichols, B.L.; Hirst, E.A.; Michel, J.W.; Yee, W.C. *Agricultural and Aquacultural Uses of Waste Heat*; Technical Report No. ORNL-4797; Oak Ridge National Lab.: Oak Ridge, TN, USA, 1972. [[CrossRef](#)]
10. Little, A.B.; Garimella, S. Comparative Assessment of Alternative Cycles for Waste Heat Recovery and Upgrade. *Energy* **2011**, *36*, 4492–4504. [[CrossRef](#)]
11. Denzer, A.; Wang, L.; Thomas, Y.; McMorro, G. Greenhouse Design with Waste Heat: Principles and Practices. In Proceedings of the Architectural Engineering Conference 2017, Oklahoma City, OK, USA, 11–13 April 2017; pp. 440–455.
12. Pearce, J.M. Industrial Symbiosis of Very Large-Scale Photovoltaic Manufacturing. *Renew. Energy* **2008**, *33*, 1101–1108. [[CrossRef](#)]
13. Andrews, R.; Pearce, J.M. Environmental and Economic Assessment of a Greenhouse Waste Heat Exchange. *J. Clean. Prod.* **2011**, *19*, 1446–1454. [[CrossRef](#)]
14. Vourdoubas, J. Possibilities of Using Industrial Waste Heat for Heating Greenhouses in Northern Greece. *J. Agric. Sci.* **2018**, *10*, 116–123. [[CrossRef](#)]
15. Tataraki, K.G.; Kavvadias, K.C.; Maroulis, Z.B. Combined Cooling Heating and Power Systems in Greenhouses. Grassroots and Retrofit Design. *Energy* **2019**, *189*, 116283. [[CrossRef](#)]
16. Yu, M.G.; Nam, Y. Feasibility Assessment of Using Power Plant Waste Heat in Large Scale Horticulture Facility Energy Supply Systems. *Energies* **2016**, *9*, 112. [[CrossRef](#)]
17. Fguiri, A.; Fatnassi, H.; Jeday, M.-R.; Marvillet, C. Study of the Energetic and the Economic Feasibility of a Heating Agricultural Greenhouse Using Industrial Waste-Heat at Low Temperatures. *Int. J. Energy Environ. Econ.* **2017**, *25*, 269–282.
18. Sandberg, M.; Risberg, M.; Ljung, A.-L.; Varagnolo, D.; Xiong, D.; Nilsson, M. A Modelling Methodology for Assessing Use of Datacenter Waste Heat in Greenhouses. In Proceedings of the Third International Conference on Environmental Science and Technology, ICOEST, Budapest, Hungary, 19–23 October 2017.
19. Pervilä, M.; Remes, L.; Kangasharju, J. Harvesting Heat in an Urban Greenhouse. In Proceedings of the First Workshop on Urban Networking, CoNEXT '12: Conference on Emerging Networking Experiments and Technologies, Nice, France, 10 December 2012; Association for Computing Machinery: New York, NY, USA, 2012; pp. 7–12.
20. Ljungqvist, H.M.; Mattsson, L.; Risberg, M.; Vesterlund, M. Data Center Heated Greenhouses, a Matter for Enhanced Food Self-Sufficiency in Sub-Arctic Regions. *Energy* **2021**, *215*, 119169. [[CrossRef](#)]
21. Cáceres, C.R.; Törnroth, S.; Vesterlund, M.; Johansson, A.; Sandberg, M. Data-Center Farming: Exploring the Potential of Industrial Symbiosis in a Subarctic Region. *Sustainability* **2022**, *14*, 2774. [[CrossRef](#)]
22. Kozai, T. Thermal Performance of an Oil Engine Driven Heat Pump for Greenhouse Heating. *J. Agric. Eng. Res.* **1986**, *35*, 25–37. [[CrossRef](#)]
23. Chinese, D.; Meneghetti, A.; Nardin, G. Waste-to-Energy Based Greenhouse Heating: Exploring Viability Conditions through Optimisation Models. *Renew. Energy* **2005**, *30*, 1573–1586. [[CrossRef](#)]
24. González-Briones, A.; Chamoso, P.; Prieto, J.; Corchado, J.M.; Yoe, H. Reuse of Wasted Thermal Energy in Power Plants for Agricultural Crops by Means of Multi-Agent Approach. In Proceedings of the 2018 International Conference on Smart Energy Systems and Technologies (SEST), Seville, Spain, 10–12 September 2018; pp. 1–6.
25. Dhiman, M.; Sethi, V.P.; Singh, B.; Sharma, A. CFD Analysis of Greenhouse Heating Using Flue Gas and Hot Water Heat Sink Pipe Networks. *Comput. Electron. Agric.* **2019**, *163*, 104853. [[CrossRef](#)]
26. Iddio, E.; Wang, L.; Thomas, Y.; McMorro, G.; Denzer, A. Energy Efficient Operation and Modeling for Greenhouses: A Literature Review. *Renew. Sustain. Energy Rev.* **2020**, *117*, 109480. [[CrossRef](#)]
27. Syed, A.M.; Hachem, C. Net-Zero Energy Design and Energy Sharing Potential of Retail-Greenhouse Complex. *J. Build. Eng.* **2019**, *24*, 100736. [[CrossRef](#)]
28. Muñoz-Liesa, J.; Royapoor, M.; Cuerva, E.; Gassó-Domingo, S.; Gabarrell, X.; Josa, A. Building-Integrated Greenhouses Raise Energy Co-Benefits through Active Ventilation Systems. *Build. Environ.* **2022**, *208*, 108585. [[CrossRef](#)]

29. Parker, T.; Kiessling, A. Low-Grade Heat Recycling for System Synergies between Waste Heat and Food Production, a Case Study at the European Spallation Source. *Energy Sci. Eng.* **2016**, *4*, 153–165. [[CrossRef](#)]
30. Luo, Y.; Andresen, J.; Clarke, H.; Rajendra, M.; Maroto-Valer, M. A Decision Support System for Waste Heat Recovery and Energy Efficiency Improvement in Data Centres. *Appl. Energy* **2019**, *250*, 1217–1224. [[CrossRef](#)]
31. Ebrahimi, K.; Jones, G.F.; Fleischer, A.S. A Review of Data Center Cooling Technology, Operating Conditions and the Corresponding Low-Grade Waste Heat Recovery Opportunities. *Renew. Sustain. Energy Rev.* **2014**, *31*, 622–638. [[CrossRef](#)]
32. Liu, J.; Goraczko, M.; James, S.; Belady, C.; Lu, J.; Whitehouse, K. The Data Furnace: Heating up with Cloud Computing. In Proceedings of the 3rd USENIX Workshop on Hot Topics in Cloud Computing, Portland, OR, USA, 14–15 June 2011.
33. Kosik, B. Data Centers Used for Bitcoin Mining: Data Centers Used for Bitcoin Mining Have Significant Differences from Their Commercial Data Center Counterparts. *Consult. Specif. Eng.* **2018**, *55*, 20–25.
34. Monetary Policy and Central Banking. Available online: <https://www.imf.org/en/About/Factsheets/Sheets/2016/08/01/16/20/Monetary-Policy-and-Central-Banking> (accessed on 30 October 2022).
35. Houy, N. The Bitcoin Mining Game. *Ledger* **2016**, *1*, 53–68. [[CrossRef](#)]
36. DeVries, P.D. An Analysis of Cryptocurrency, Bitcoin, and the Future. *Int. J. Bus. Manag. Commer.* **2016**, *1*, 1–9.
37. Nakamoto, S. Bitcoin: A Peer-to-Peer Electronic Cash System. *Decentralized Bus. Rev.* **2008**, *1*, 21260.
38. Market Capitalization of Bitcoin (BTC) from April 2013 to 8 August 2022. Available online: <https://www.statista.com/statistics/377382/bitcoin-market-capitalization/> (accessed on 30 October 2022).
39. Ankalkoti, P.; Santhosh, S.G. A Relative Study on Bitcoin Mining. *Imp. J. Interdiscip. Res.* **2017**, *3*, 1757–1761.
40. Dimitri, N. Bitcoin Mining as a Contest. *Ledger* **2017**, *2*, 31–37. [[CrossRef](#)]
41. Kroll, J.A.; Davey, I.C.; Felten, E.W. The Economics of Bitcoin Mining, or Bitcoin in the Presence of Adversaries. In Proceedings of the WEIS, Washington, DC, USA, 11–12 June 2013; Volume 2013.
42. Dhumwad, S.; Sukhadeve, M.; Naik, C.; Manjunath, K.N.; Prabhu, S. A Peer to Peer Money Transfer Using SHA256 and Merkle Tree. In Proceedings of the 2017 23rd Annual International Conference in Advanced Computing and Communications (ADCOM), Bangalore, India, 8–10 September 2017; pp. 40–43.
43. Bhaskar, N.D.; Chuen, D.L.E.E.K. Chapter 3—Bitcoin Mining Technology. In *Handbook of Digital Currency*; Lee Kuo Chuen, D., Ed.; Academic Press: San Diego, CA, USA, 2015; pp. 45–65; ISBN 978-0-12-802117-0.
44. Liu, Y.; Chen, X.; Zhang, L.; Tang, C.; Kang, H. An Intelligent Strategy to Gain Profit for Bitcoin Mining Pools. In Proceedings of the 2017 10th International Symposium on Computational Intelligence and Design (ISCID), Hangzhou, China, 9–10 December 2017; Volume 2, pp. 427–430.
45. Castilla, N. *Greenhouse Technology and Management*, 2nd ed.; CABI Publishing: Oxfordshire, UK, 2013; ISBN 9781780641034.
46. Singh, R.D.; Tiwari, G.N. Energy Conservation in the Greenhouse System: A Steady State Analysis. *Energy* **2010**, *35*, 2367–2373. [[CrossRef](#)]
47. Sethi, V.P. On the Selection of Shape and Orientation of a Greenhouse: Thermal Modeling and Experimental Validation. *Sol. Energy* **2009**, *83*, 21–38. [[CrossRef](#)]
48. Rogers Greenhouse. Available online: <http://www.rogersgreenhouse.com/> (accessed on 4 November 2022).
49. NSRDB: National Solar Radiation Database. Available online: <https://nsrdb.nrel.gov/> (accessed on 4 November 2022).
50. Crawford, C.B.; Legget, R.F. Ground Temperature Investigations in Canada. *Eng. J.* **1957**, *40*, 263–269, 290.
51. Tomato. Land & Water. Food and Agriculture Organization of the United Nations. Available online: <https://www.fao.org/land-water/databases-and-software/crop-information/tomato/en/> (accessed on 31 May 2022).
52. Bakker, J.C.; Bot, G.P.A.; Challa, H.; Van de Braak, N.J. *Greenhouse Climate Control: An Integrated Approach*; Wageningen Academic Publishers: Wageningen, The Netherlands, 1995; ISBN 978-90-8686-501-7.
53. Bambara, J. A Methodology for the Design of Greenhouses with Semi-Transparent Photovoltaic Cladding and Artificial Lighting. Ph.D. Thesis, Concordia University, Montreal, QC, Canada, 2018.
54. Choab, N.; Allouhi, A.; Maakoul, A.E.; Kousksou, T.; Saadeddine, S.; Jamil, A. Effect of Greenhouse Design Parameters on the Heating and Cooling Requirement of Greenhouses in Moroccan Climatic Conditions. *IEEE Access* **2021**, *9*, 2986–3003. [[CrossRef](#)]
55. Mohsenipour, M.; Ebadollahi, M.; Rostamzadeh, H.; Amidpour, M. Design and Evaluation of a Solar-Based Trigeneration System for a Nearly Zero Energy Greenhouse in Arid Region. *J. Clean. Prod.* **2020**, *254*, 119990. [[CrossRef](#)]
56. Mahmood, F.; Al-Ansari, T.A. Design and Thermodynamic Analysis of a Solar Powered Greenhouse for Arid Climates. *Desalination* **2021**, *497*, 114769. [[CrossRef](#)]
57. Sethi, V.P.; Sharma, S.K. Thermal Modeling of a Greenhouse Integrated to an Aquifer Coupled Cavity Flow Heat Exchanger System. *Sol. Energy* **2007**, *81*, 723–741. [[CrossRef](#)]
58. Başak, M.Z.; Sevilgen, S.H. A Techno-Economic Model for Heating of a Greenhouse Site Using Waste Heat. *Arab. J. Sci. Eng.* **2016**, *41*, 1895–1905. [[CrossRef](#)]
59. Aldrich, R.A.; Bartok, J.W. *Greenhouse Engineering (NRAES 33)*; Northeast Regional Agricultural Engineering Service (NRAES): College Park, MD, USA, 1994.
60. Crypto Mining Container For Sale | Fastest Mining Container Delivery—Call 1.780.482.6838. Available online: <https://bit-ram.ca/> (accessed on 25 November 2022).

61. Pzem-022 + PEACEFAIR PZEM-022 AC Digital Meter Power Energy Voltage Current Test With Closed Type CT 100A: Amazon.ca: Tools & Home Improvement. Available online: <https://www.amazon.ca/PEACEFAIR-PZEM-022-Digital-Voltage-Current/dp/B07YZJ2D6G> (accessed on 25 November 2022).
62. McDonald, M.T.; Hayibo, K.S.; Hafting, F.; Pearce, J.M. Economics of Open-Source Solar Photovoltaic Powered Cryptocurrency Mining. *SSRN Electron. J.* **2022**. [CrossRef]
63. FLIR C5 Compact Thermal Camera with Cloud Connectivity and Wi-Fi. Teledyne FLIR. Available online: <https://www.flir.ca/products/c5/?vertical=condition+monitoring&segment=solutions> (accessed on 25 November 2022).
64. Bitcoin Price Chart and Tables. Finance Reference. Available online: <https://www.in2013dollars.com/bitcoin-price> (accessed on 25 November 2022).
65. Electricity Prices in Canada 2021. Available online: <https://www.energyhub.org/electricity-prices/> (accessed on 25 November 2022).
66. Electricity Cost in Texas: 2022 Electric Rates. EnergySage. Available online: <https://www.energysage.com/local-data/electricity-cost/tx/> (accessed on 25 November 2022).
67. Electricity Cost in California: 2022 Electric Rates. EnergySage. Available online: <https://www.energysage.com/local-data/electricity-cost/ca/> (accessed on 25 November 2022).
68. Electricity Cost in New York: 2022 Electric Rates. EnergySage. Available online: <https://www.energysage.com/local-data/electricity-cost/ny/> (accessed on 25 November 2022).
69. Ahamed, M.S.; Guo, H.; Taylor, L.; Tanino, K. Heating Demand and Economic Feasibility Analysis for Year-Round Vegetable Production in Canadian Prairies Greenhouses. *Inf. Process. Agric.* **2019**, *6*, 81–90. [CrossRef]
70. Amazon.Com: W12E12BS11B5-57 12 V 1.65 A 120 mm L × 120 mm W × 38 mm H Cabinet Cooling Fan: Electronics. Available online: <https://www.amazon.com/Bomin-Technology-W12E12BS11B5-07-4-Wire-Cooling/dp/B0866D8LKX> (accessed on 25 November 2022).
71. Bill Calculator. Ontario Energy Board. Available online: <https://www.oeb.ca/consumer-information-and-protection/bill-calculator> (accessed on 3 December 2022).
72. Understand Your Bill. Business. Énergir. Available online: <https://www.energir.com/en/business/customer-centre/billing-and-pricing/understanding-your-bill/> (accessed on 3 December 2022).
73. Utilities Consumer Advocate—Compare Your Energy Choices. Available online: <https://ucahelps.alberta.ca/cost-comparison-tool-detailed.aspx?usageType=1&energyType=energyTypeNeither&locationCityTown=&locationPostalCode=t3L+1v1&locationMeterNumber=&locationCityTownPostal=&locationSiteID=&naturalGasMonth=&electricityUsage=&electricityBillingDemand=&electricityFarmUsage=&naturalGasUsage=&planIDs=16120> (accessed on 5 December 2022).
74. New York Price of Natural Gas Delivered to Residential Consumers (Dollars per Thousand Cubic Feet). Available online: <https://www.eia.gov/dnav/ng/hist/n3010ny3A.htm> (accessed on 3 December 2022).
75. Tahery, D.; Roshandel, R.; Avami, A. An Integrated Dynamic Model for Evaluating the Influence of Ground to Air Heat Transfer System on Heating, Cooling and CO₂ Supply in Greenhouses: Considering Crop Transpiration. *Renew. Energy* **2021**, *173*, 42–56. [CrossRef]
76. Ouazzani Chahidi, L.; Fossa, M.; Priarone, A.; Mechaqrane, A. Greenhouse Cultivation in Mediterranean Climate: Dynamic Energy Analysis and Experimental Validation. *Therm. Sci. Eng. Prog.* **2021**, *26*, 101102. [CrossRef]
77. Dong, S.; Ahamed, M.S.; Ma, C.; Guo, H. A Time-Dependent Model for Predicting Thermal Environment of Mono-Slope Solar Greenhouses in Cold Regions. *Energies* **2021**, *14*, 5956. [CrossRef]
78. Agriculture and Agri-Food Canada - Agriculture.Canada. Available online: <https://agriculture.canada.ca/en> (accessed on 25 January 2023).
79. Russia Is a Major Supplier of Oil to the U.S. Available online: <https://www.forbes.com/sites/rpapier/2022/02/21/russia-is-a-major-supplier-of-oil-to-the-us/?sh=4a3c5ef718c3> (accessed on 3 December 2022).
80. United States Inflation Rate—November 2022 Data—1914–2021 Historical. Available online: <https://tradingeconomics.com/united-states/inflation-cpi> (accessed on 3 December 2022).
81. Garriga, C.; Werner, D. Inflation, Part 3: What Is the Fed’s Current Goal? Has the Fed Met Its Inflation Mandate? *Econ. Synopses* **2022**, *2022*, 1–3. [CrossRef]
82. Federal Reserve Interest Rates and How They Affect You. The Ascent by Motley Fool. Available online: <https://www.fool.com/the-ascent/federal-reserve-interest-rates/> (accessed on 3 December 2022).
83. Dow Dives 800 Points, S&P 500 Posts Worst Week since January after Inflation Hits 40-Year High. Available online: <https://www.cnbc.com/2022/06/09/stock-market-news-open-to-close.html> (accessed on 3 December 2022).
84. Dinesh, H.; Pearce, J.M. The Potential of Agrivoltaic Systems. *Renew. Sustain. Energy Rev.* **2016**, *54*, 299–308. [CrossRef]
85. Allardyce, C.S.; Fankhauser, C.; Zakeeruddin, S.M.; Grätzel, M.; Dyson, P.J. The Influence of Greenhouse-Integrated Photovoltaics on Crop Production. *Sol. Energy* **2017**, *155*, 517–522. [CrossRef]
86. Li, C.; Wang, H.; Miao, H.; Ye, B. The Economic and Social Performance of Integrated Photovoltaic and Agricultural Greenhouses Systems: Case Study in China. *Appl. Energy* **2017**, *190*, 204–212. [CrossRef]
87. Nayak, S.; Tiwari, G.N. Theoretical Performance Assessment of an Integrated Photovoltaic and Earth Air Heat Exchanger Greenhouse Using Energy and Exergy Analysis Methods. *Energy Build.* **2009**, *41*, 888–896. [CrossRef]
88. Pearce, J.M. Agrivoltaics in Ontario Canada: Promise and Policy. *Sustainability* **2022**, *14*, 3037. [CrossRef]

89. Dual Use for Solar Modules—Greenhouse Canada. Available online: <https://www.greenhousecanada.com/technology-issues-dual-use-for-solar-modules-32902/> (accessed on 25 November 2022).
90. Growing Trial for Greenhouse Solar Panels—Research & Innovation. Niagara College. Available online: <https://www.ncinnovation.ca/blog/research-innovation/growing-trial-for-greenhouse-solar-panels> (accessed on 25 November 2022).
91. Pearce, J.M. Parametric Open Source Cold-Frame Agrivoltaic Systems. *Inventions* **2021**, *6*, 71. [CrossRef]
92. El-Bashir, S.M.; Al-Harbi, F.F.; Elburaih, H.; Al-Faifi, F.; Yahia, I.S. Red Photoluminescent PMMA Nanohybrid Films for Modifying the Spectral Distribution of Solar Radiation inside Greenhouses. *Renew. Energy* **2016**, *85*, 928–938. [CrossRef]
93. Increasing Yield Using High-Tech Greenhouse Film. UbiGro. Available online: <https://ubigro.com/case-studies/> (accessed on 25 November 2022).
94. Parrish, C.H.; Hebert, D.; Jackson, A.; Ramasamy, K.; McDaniel, H.; Giacomelli, G.A.; Bergren, M.R. Optimizing Spectral Quality with Quantum Dots to Enhance Crop Yield in Controlled Environments. *Commun. Biol.* **2021**, *4*, 124. [CrossRef]
95. OSF. Available online: <https://osf.io/exnj7/files/osfstorage> (accessed on 5 December 2022).
96. Duffie, J.A.; Beckman, W.A. *Solar Engineering of Thermal Processes*, 4th ed.; John Wiley & Sons: Hoboken, NJ, USA, 2013.
97. Ahamed, M.S.; Guo, H.; Tanino, K. Energy Saving Techniques for Reducing the Heating Cost of Conventional Greenhouses. *Biosyst. Eng.* **2019**, *178*, 9–33. [CrossRef]
98. Macrolux Multiwall—Macrolux. Available online: <https://www.macroluxusa.com/macrolux-multiwall> (accessed on 2 July 2022).
99. Palmitezza, O.D.; Pantaleo, M.A.; Santamaria, P. Applications and Development of LEDs as Supplementary Lighting for Tomato at Different Latitudes. *Agronomy* **2021**, *11*, 835. [CrossRef]
100. DLI Calculator. SunTracker Technologies Ltd. Available online: <https://www.suntrackertech.com/dli-calculator/> (accessed on 4 July 2022).
101. Singh, D.; Basu, C.; Meinhardt-Wollweber, M.; Roth, B. LEDs for Energy Efficient Greenhouse Lighting. *Renew. Sustain. Energy Rev.* **2015**, *49*, 139–147. [CrossRef]
102. Bambara, J.; Athienitis, A.K. Energy and Economic Analysis for Greenhouse Envelope Design. *Trans. ASABE* **2018**, *61*, 1795–1810. [CrossRef]
103. Ashrae. *ASHRAE Handbook of Fundamentals, SI Edition*; American Society of Heating Ventilation Refrigeration and Air-conditioning Engineers: Atlanta, GA, USA, 2013.
104. Bergman, T.L.; Lavine, A.S.; Incropera, F.P.; DeWitt, D.P. *Introduction to Heat Transfer*, 6th ed.; John Wiley & Sons: Hoboken, NJ, USA, 2011.
105. Pieters, J.G.; Deltour, J.M. Performances of Greenhouses with the Presence of Condensation on Cladding Materials. *J. Agric. Eng. Res.* **1997**, *68*, 125–137. [CrossRef]
106. Boccalatte, A.; Fossa, M.; Sacile, R. Modeling, Design and Construction of a Zero-Energy PV Greenhouse for Applications in Mediterranean Climates. *Therm. Sci. Eng. Prog.* **2021**, *25*, 101046. [CrossRef]
107. Watson, J.A.; McConnell, D.B.; Henley, R.W.; Gomez, C.; Bucklin, R.A. *Greenhouse Ventilation*; EDIS: Gainesville, FL, USA, 2019.
108. Yildirim, N.; Bilir, L. Evaluation of a Hybrid System for a Nearly Zero Energy Greenhouse. *Energy Convers. Manag.* **2017**, *148*, 1278–1290. [CrossRef]
109. Ben Ali, R.; Bouadila, S.; Mami, A. Experimental Validation of the Dynamic Thermal Behavior of Two Types of Agricultural Greenhouses in the Mediterranean Context. *Renew. Energy* **2020**, *147*, 118–129. [CrossRef]
110. Ahamed, M.S.; Guo, H.; Tanino, K. Energy-Efficient Design of Greenhouse for Canadian Prairies Using a Heating Simulation Model. *Int. J. Energy Res.* **2018**, *42*, 2263–2272. [CrossRef]
111. Mohammadi, B.; Ranjbar, F.; Ajabshirchi, Y. Exergoeconomic Analysis and Multi-Objective Optimization of a Semi-Solar Greenhouse with Experimental Validation. *Appl. Therm. Eng.* **2020**, *164*, 114563. [CrossRef]
112. Nobel, P.S. *Introduction to Biophysical Plant Physiology*; W.H. Freeman and Company: San Francisco, CA, USA, 1970.
113. Boulard, T.; Wang, S. Greenhouse Crop Transpiration Simulation from External Climate Conditions. *Agric. For. Meteorol.* **2000**, *100*, 25–34. [CrossRef]

Disclaimer/Publisher’s Note: The statements, opinions and data contained in all publications are solely those of the individual author(s) and contributor(s) and not of MDPI and/or the editor(s). MDPI and/or the editor(s) disclaim responsibility for any injury to people or property resulting from any ideas, methods, instructions or products referred to in the content.